

Chapter 9

The Muon Storage Ring Magnet

9.1 Introduction

As emphasized in Chapter 2, the determination of the muon anomaly a_μ requires a precise measurement of the muon spin frequency in a magnetic field ω_a , and an equally precise measurement of the average magnetic field felt by the ensemble of precessing muons, $\langle B \rangle$. We repeat the spin equation given in Eq. 3.10, since it is central to the design of the storage-ring magnet.

$$\vec{\omega}_a = -\frac{Qe}{m} \left[a_\mu \vec{B} - \left(a_\mu - \left(\frac{mc}{p} \right)^2 \right) \frac{\vec{\beta} \times \vec{E}}{c} \right]. \quad (9.1)$$

As explained in Chapter 2, the need for vertical focusing and exquisite precision on $\langle B \rangle$ requires that: either the muon trajectories be understood at the tens of parts per billion level, and the magnetic field everywhere be known to the same precision; or the field be as uniform as possible and well-measured, along with “reasonable knowledge” of the muon trajectories. This latter solution was first employed at CERN [1] and significantly improved by E821 at Brookhaven [2]. The uniformity goal at BNL was ± 1 ppm when averaged over azimuth, with local variations limited to ≤ 100 ppm.

Fermilab E989 will use the storage-ring magnet designed and built for Brookhaven E821, with additional shimming to further decrease the local variations in the magnetic field. This requires the relocation of the ring from BNL to Fermilab, which is described in detail in the following chapter. While the magnet steel comes apart and can be moved by conventional trucks, the 14.5 m diameter superconducting coils will need to be moved as a package, on a custom designed fixture that can be pulled by a truck to travel by road, and put on a barge to travel by sea, and then again by road to get it to the Fermilab site.

The storage ring is built as one continuous superferric magnet, an iron magnet excited by superconducting coils. A cross-section of the magnet is shown in Fig. 9.1. The magnet is C-shaped as dictated by the experiment requirement that decay electrons be observed inside the ring. The field, and hence its homogeneity and stability, are determined dominantly by the geometry, characteristics, and construction tolerances of the iron. Although both copper and superconducting coils were considered, the use of superconducting coils offered the following advantages: thermal stability once cold; relatively low power requirements; low voltage, and hence use of a low-voltage power supply; high L/R time constant value

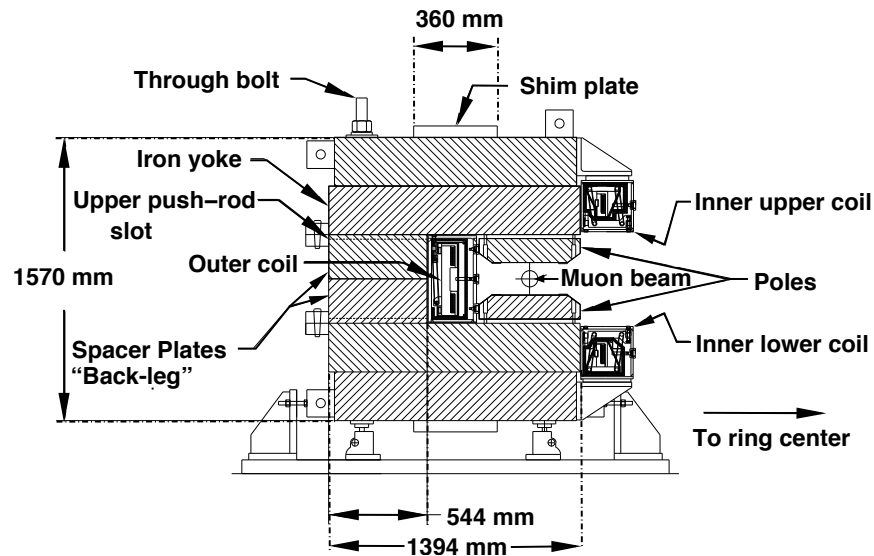


Figure 9.1: Cross section of the E821 storage-ring magnet. The yoke is made up of 12 azimuthal sections, each of which consists of six layers of high quality magnet steel provided by Lukins Steel Corporation. The pole pieces were provided by Nippon Steel Corporation.

and hence low ripple currents; and thermal independence of the coils and the iron. The main disadvantage was that the coils would have a much larger diameter and smaller height than any previously built superconducting magnet. However, since the E821 magnet team could not identify any fundamental problems other than sheer size, they decided to build superconducting coils.

To obtain the required precision in such a large diameter magnet with an economical design is an enormous challenge. The magnet had to be a mechanical assembly from sub-pieces because of its size. With practical tolerances on these pieces, variations up to several thousand ppm in the magnetic field could be expected from the assembled magnet. To improve this result by the required two to three orders of magnitude required a shimming kit.

Because of the dominant cost of the yoke iron, it was an economic necessity to minimize the total flux and the yoke cross-section. This led to a narrow pole, which in turn conflicts with producing an ultra-uniform field over the 9 cm good field aperture containing the muon beam.

A simple tapered pole shape was chosen which minimized variations in the iron permeability and field throughout the pole. The ratio of pole tip width to gap aperture is only 2/1. This results in a large dependence of the field shape with the field value B . However, since the storage ring is to be used at only one field, $B = 1.45$ T, this is acceptable. Because of dimensional and material property tolerance variation, the compact pole piece increases the necessity for a simple method of shimming.

Experience with computer codes, in particular with POISSON [4], had demonstrated that, with careful use, agreement with experiment could be expected at a level of 10^{-4} accuracy. POISSON is a two-dimensional (2D) or cylindrically symmetric code, appropriate for the essen-

tially continuous ring magnet chosen for the $(g - 2)$ experiment. Computational limitations, finite boundary conditions, and material property variations are all possible limitations on the accuracy of paper calculations of the design.

We will briefly discuss the design features that are relevant to E989, especially to moving the ring, but not repeat all the details given in Danby et al. [3], and in the E821 Design Report [5]. The parameters of the magnet are given in Table 9.1.

Table 9.1: Magnet parameters

| | |
|-------------------------------|-----------------|
| Design magnetic field | 1.451 T |
| Design current | 5200 A |
| Equilibrium orbit radius | 7112 mm |
| Muon storage region diameter | 90 mm |
| Inner coil radius - cold | 6677 mm |
| Inner coil radius - warm | 6705 mm |
| Outer coil radius - cold | 7512 mm |
| Outer coil radius - warm | 7543 mm |
| Number of turns | 48 |
| Cold mass | 6.2 metric tons |
| Magnet self inductance | 0.48 H |
| Stored energy | 6.1 MJ |
| Helium-cooled lead resistance | $6 \mu\Omega$ |
| Warm lead resistance | 0.1 m Ω |
| Yoke height | 157 cm |
| Yoke width | 139 cm |
| Pole width | 56 cm |
| Iron mass | 682 metric tons |
| Nominal gap between poles | 18 cm |

9.2 Yoke Steel

E989 will reuse the yoke steel manufactured for the E821 experiment. The yoke pieces have been surveyed and disassembled at Brookhaven and have been shipped to Fermilab. The design and construction of the magnet has been documented and published in NIM [3] as well as the final report in Phys. Rev. D [2]. We summarize the main design features and issues here, with a discussion of potential improvements in Section 9.4.

Ideally, the $g - 2$ magnet would be azimuthally symmetric. To ease the fabrication and assembly processes, the magnet was built with twelve 30° sectors. Each sector consists of an upper and lower yoke separated by a spacer plate as shown in Fig. 9.1. Due to the large thickness of the yoke (54 cm), the individual plates were fabricated separately and welded together after machining. The spacer plate is also split at the midplane to allow for the installation of beam pipes and other services after the lower section is in place but prior to

the installation of the upper yoke. The yoke plates and spacers in each sector are all fastened together with eight long high-strength steel bolts that cover the full 1.57 m tall yoke. The total sector mass is $\approx 57,000$ kg, which results in a total magnet mass of $\approx 680,000$ kg.

Significant quality control efforts were taken during the manufacturing process to ensure that the magnet had sufficiently uniform permeability and the appropriate geometric shape. Both of these parameters have strong effects on the uniformity of the magnetic field in the storage region.

High-quality plates were manufactured by hot-rolling AISI 1006 iron to minimize magnetic voids in the material. These plates were manufactured with $< 0.08\%$ of carbon and other impurities. The finished plates were inspected ultrasonically to detect voids and inclusions, and analyzed chemically to understand the composition.

Although the yoke steel is partially magnetically isolated from the storage region by an air gap near the pole pieces, strict machining specifications are required to minimize non-uniformities in the storage region field. The surfaces of the yoke plates closest to the storage region were milled flat within $130\ \mu\text{m}$ and $1.6\ \mu\text{m}$ finish. Similarly, the spacer plate surfaces were milled flat within $\pm 130\ \mu\text{m}$, with a thickness accurate to $\pm 130\ \mu\text{m}$. These surfaces are parallel within $180\ \mu\text{m}$. The radial tolerance for each yoke plate and the spacer plates was $\pm 130\ \mu\text{m}$. When constructed, the vertical yoke gap had an rms deviation of $\pm 90\ \mu\text{m}$, or 500 ppm of the total air gap of 20 cm, and a full-width spread of $\pm 200\ \mu\text{m}$.

Each of the 12 sectors need to be connected smoothly to achieve azimuthal symmetry. To achieve azimuthal continuity, each sector end has four radial projections for bolts to fasten adjacent sector ends to each other. When the sectors are fitted to each other, shimmed, and the bolts tightened, relative motion of adjacent sectors is minimized. The average azimuthal gap between sectors was 0.8 mm, with an rms deviation of ± 0.2 mm.

When we begin to reconstruct the storage ring, we will clean the yoke steel and remove any rust that has developed. It will be important to do this in a non-destructive manner that maintains the high-level of precision achieved during manufacturing.

9.3 Poles and Wedges

E989 will reuse the pole pieces and wedge shims that were manufactured for the E821 experiment. The pole pieces and wedges have been removed from the storage ring at Brookhaven and have already been shipped to Fermilab where they are awaiting reassembly.

9.3.1 Poles

More stringent quality requirements are placed on the machining of the pole pieces than the yoke steel. The air gap between the yoke and pole pieces decouples the field region from non-uniformities in the yoke. Thus, irregularities in the pole pieces dominate the field aberrations. Ultra-pure continuous vacuum cast steel with $< 0.004\%$ carbon impurities is used for the pole pieces. The fabrication process greatly minimizes impurities such as ferritic inclusions or air bubbles.

A dimensioned view of the pole pieces is shown in Figure 9.2. Each 30° yoke sector contains three pole pieces (azimuthally). The pole pieces are 56 cm wide (radially), with

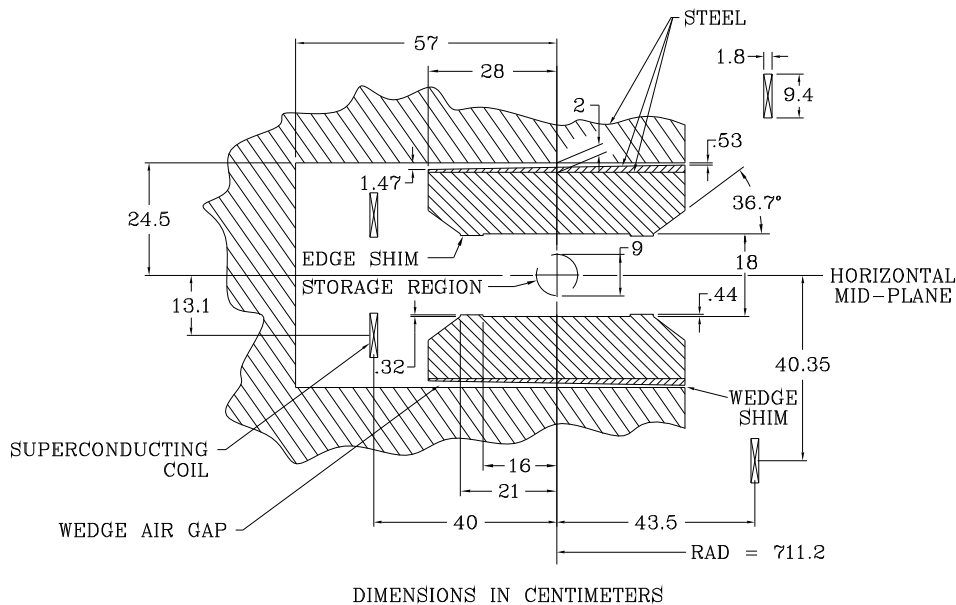


Figure 9.2: Cross section view of the magnet gap region.

a tolerance of $50\ \mu\text{m}$. The thickness (vertical) of each piece is $13.3\ \text{cm}$ with a tolerance of $40\ \mu\text{m}$. The pole faces which define the storage ring gap have tight machining tolerances. Each face has a flatness tolerance of $25\ \mu\text{m}$, leading to upper and lower faces being parallel within a $50\ \mu\text{m}$ tolerance. The surface finish is $0.8\ \mu\text{m}$. These machining tolerances are so stringent due to the large quadrupole moment introduced by non-parallel surfaces. An OPERA-2D simulation of the magnet has determined that a $100\ \mu\text{m}$ tilt of the pole piece over its width corresponds to $> 100\ \text{ppm}$. This is in good agreement with the 2D POISSON calculations performed for the E821 simulations.

Each yoke sector contains three pole pieces. Vertically, the pole pieces are mounted to the yoke plates with steel bolts. The outer two pieces are each machined radially, parallel to the yoke sector. The middle pole piece in each sector is interlocking, with an angle of 7° with respect to the radial direction. The pole pieces were isolated azimuthally by $80\ \mu\text{m}$ kapton shims, which served two purposes. First, the kapton shims helped position the pole pieces at the correct azimuth. Second, the kapton electrically isolated the poles from each other, allowing small reproducible eddy currents. If the poles were all in contact with each other, large eddy currents would develop around the entire circumference of the ring during field ramping and energy extraction.

The pole gap distance was measured using a capacitive sensor, as described in Section 15.8.2. The gap was $18\ \text{cm}$ with an rms variation of $\pm 23\ \mu\text{m}$, and a full range of $130\ \mu\text{m}$. As the magnet is powered, the induced torque causes the open side of the C-magnet (inner

radius) to close slightly. Thus, during the installation, the poles were aligned with an opening angle of $80 \mu\text{rad}$. A precise bubble level was used to achieve $50 \mu\text{m}$ precision over the length of the pole piece. Pole realignment will be part of the shimming process described in Section 15.8.2.

9.3.2 Wedges

The gaps between the yoke and poles isolate the yoke steel from the poles and provide a region where shims can be inserted to fine-tune the magnetic field. Steel wedges that are sloped radially (see Fig 9.2) are inserted to compensate for the intrinsic quadrupole moment produced by the C-magnet. There are 72 wedges in each 30° yoke sector. The induced quadrupole term depends on the slope of the wedge, which was calculated to be 1.1 cm over the 53 cm width for E821. This wedge angle was verified empirically, and no additional grinding was needed. The radial position of the wedges can be adjusted to change the total material in the gap, affecting only the dipole moment (see Section 15.8.3).

During the ramping of the main coil current, the thick end of the wedge attracts more field lines, leading to a torque. To prevent the wedges from deflecting vertically, an aluminum “anti-wedge” is used to fill the air gap between the wedge and the pole piece.

E989 will reuse the wedge-spacer combination as is. Fine tuning of the quadrupole moment can be achieved with active current shims, and pole bumps, as discussed in Section 15.8.3.

9.4 Thermal Effects

Temperature variations in the experimental hall are expected to be controlled within $\pm 1^\circ\text{C}$ during the course of data taking. This will change the shape of the magnet, which will in turn change the magnetic field. We produced thermal simulations with ANSYS to quantify the geometric distortions, which are then input into the OPERA-2D model of the storage ring.

E821 used 3.5” of fiber glass insulation around the bulk of the yoke and 3/8” foam rubber insulation near the poles pieces, as shown in Figure 9.3 (a). Reasonable thermal film coefficients in the range of 5-25 $\text{W}/\text{m}^2\text{C}$ were used at the surfaces of the magnet. Thermal oscillations based on day-night temperature cycles are imposed on the $g - 2$ magnet system and modeled with ANSYS. The air temperature is assumed to be spatially uniform throughout the hall. The model indicates that this will lead to thermal fluctuations at the yoke and pole pieces of a few tenths of a degree, as shown in Figure 9.3 (b). The pole pieces are constrained mechanically to prevent sliding, thus, in response to the thermal variations, they bend.

Figure 9.4 shows the response of the magnet under the 1°C hall fluctuations. The contours show the maximum extent of the deflection for both radial shifts (Figure 9.4 (a)) and vertical shifts (Figure 9.4 (b)). The deflections are on the order of $1 \mu\text{m}$ per degree C change in the hall temperature. The parallelism of the pole faces is known to affect the higher-order multipole components of the magnetic field. Figure 9.5 plots the relative change in the pole gap as a function of radius for the thermal changes described above.

Two different thermal contact resistances of the pole foam rubber insulation were modeled. In both cases, the gap distortion leads to a change of about $1 \mu\text{m}$. The pole gap

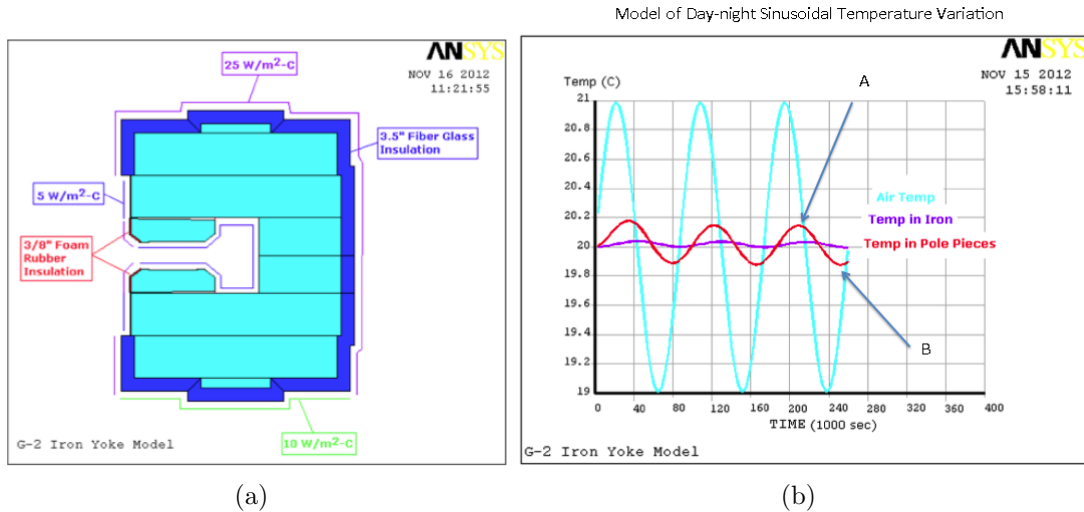


Figure 9.3: (a) An ANSYS model of the $g-2$ storage ring includes the thermal insulation used in E821. (b) Thermal oscillations based on day-night temperature cycles are imposed on the $g-2$ magnet system assuming a $\pm 1^\circ\text{C}$. The temperature variations of the yoke (purple) and pole (red) are overlaid.

distortions were input into the OPERA-2D magnetic field simulation. Distortions on the order of a few tenths of a ppm were observed in the sextupole and octupole moment with a change of $1\ \mu\text{m}$ in the pole gap. Because the monitoring of the higher order multipole moments is done primarily with the trolley runs, extrapolation of the field map from the fixed probes during the main data collection will rely on stable magnet geometry.

The ANSYS and OPERA tools nicely complement each other and allow us to understand the effects of magnet deflections in E989. We plan to repeat these studies with varied insulation thickness and with additional insulation around the inner superconducting coils. With a high quality temperature control system stabilizing the experimental hall and better thermal isolation of the steel, E989 will have significantly smaller time-dependent magnet distortions than E821. This will lead to more stable multipole components.

9.5 The Superconducting Coil System

9.5.1 Overview

The coil design was based on the TOPAZ solenoid at KEK [6]. TOPAZ conductor was used, with pure aluminum stabilizer and niobium-titanium superconductor in a copper matrix. Conductor characteristics are given in Table 9.5.1. At full field the critical temperature of the outer coil is 6.0 K. The magnet typically operates at 5.0 K. This represents 76% of the superconductor limit. Each coil block is effectively a very short solenoid with 24 turns, and one layer. The coils are wound from the inside of the ring so that, when powered, the coils push out radially against a massive aluminum mandrel. Cooling is indirect with helium pipes attached to the mandrels. The coil turns, coil stack and insulation are epoxied

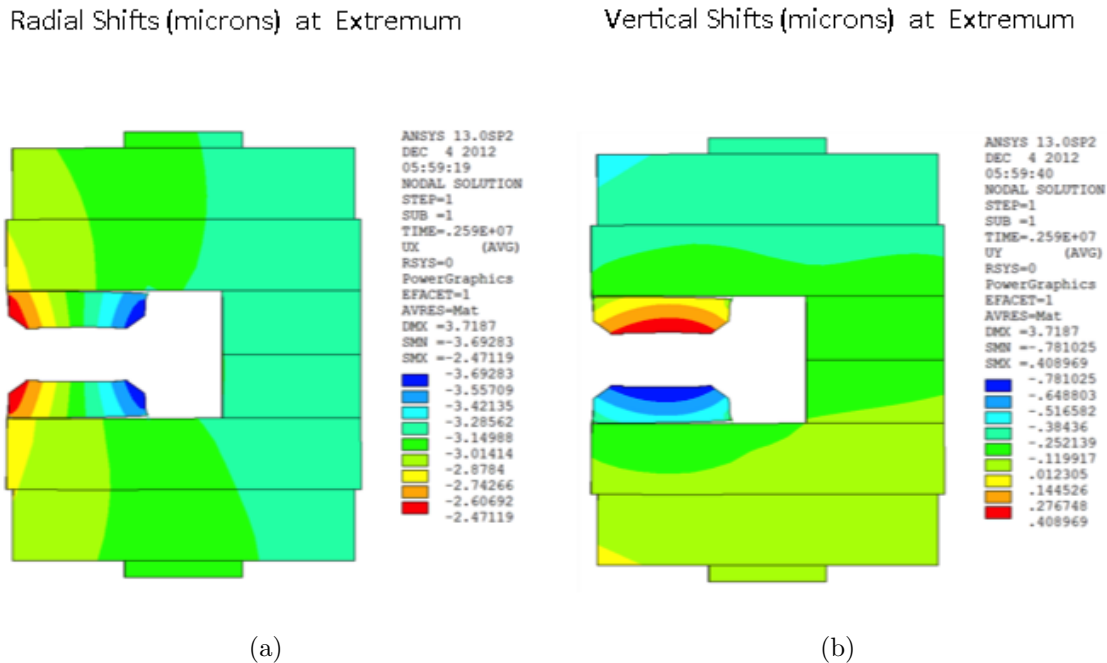


Figure 9.4: The thermal fluctuations depicted in Figure 9.3 are imposed on the magnet, causing distortion of the magnet, as modeled in ANSYS. The deflections are decomposed in (a) the radial and (b) the vertical dimensions for the worst-case scenario.

together, forming a monolithic block. The coils hang from the cryostat with low heat load straps, and the shrinkage and expansion of the coils is taken by the straps. The coils are located using radial stops on the inner radius. For the outer coil the stops transfer the force from the coil to the cryostat box, and push rods from the iron yoke transfer the force from the box to the iron (see Fig. 9.7). For the inner coils, pins replace the pushrods.

When the coils are cooled, they contract down onto the radial stops into a scalloped shape. When powered, the Lorentz force pushes the coils outward, increasing the force against the mandrel, which provides cooling. This feature, the result of winding on the inside of the mandrel, reduces the risk of cooling problems even if the coil were to separate from the mandrel during transport [7].

A ground plane insulation band of 0.3 mm thickness was built from a sandwich of three layers of 50 μm kapton, epoxy coated, between two layers of epoxy-filled fiberglass. The insulation assembly was fully cured and placed into the mandrel. A 0.1-mm layer of B-stage epoxy film was placed between the mandrel and kapton laminate, and between the kapton laminate and the conductor block after winding. A 4.8-mm thick G-10 piece was placed on the winding ledge, and on top and on the inner radius of the completed coil block. The epoxy-filled fiberglass in the ground plane insulation sandwich improved heat transfer between coil and mandrel.

The coil was then wound using a machine that wrapped the superconductor with three overlapping layers of 25 μm of kapton and fiberglass filled with B-stage epoxy, 19 mm in width, laying the conductor into the mandrel with a compressive load as described in Ref. [3].

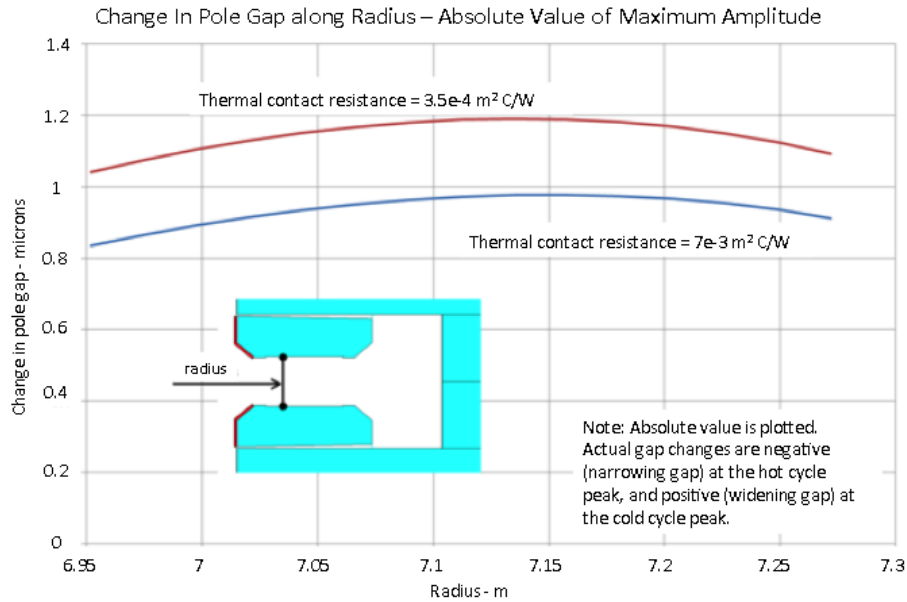


Figure 9.5: The deflections of the pole pieces under thermal variations are quantified in ANSYS simulations as a function of the radial coordinate. Typical fluctuations of 1 °C will produce micron scale distortions. Two different thermal contact resistances are shown.

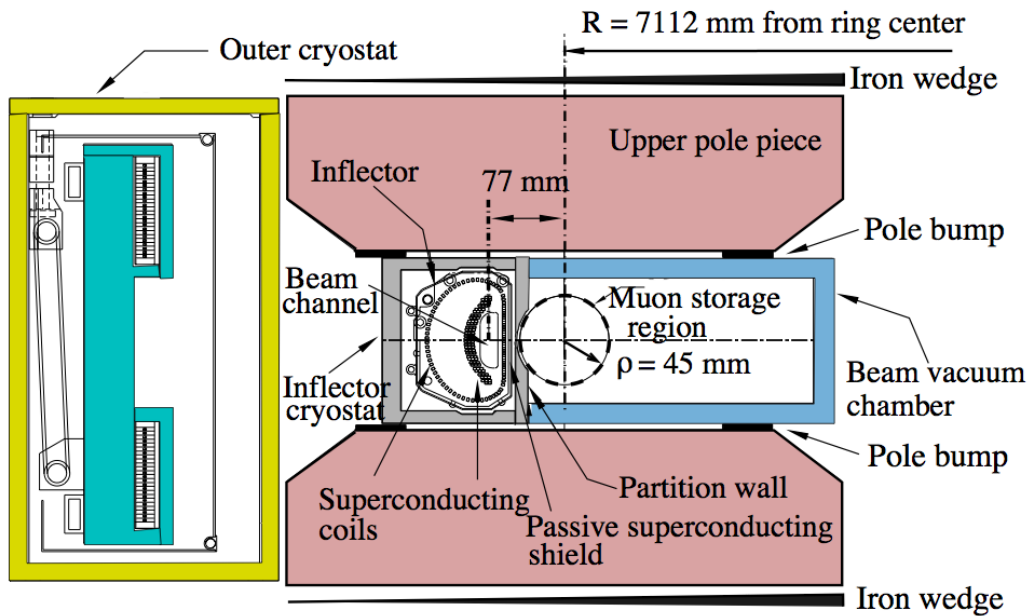


Figure 9.6: The arrangement of the pole pieces, shimming wedges and the inflector cryostat, showing the downstream end of the inflector where the beam exits. The beam is going into the page, and the ring center is to the right.

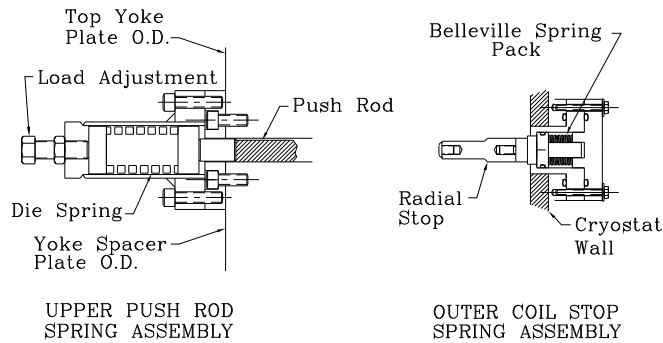


Figure 9.7: The spring-loaded radial stop and push rod. The stops are attached to the cryostat inner wall. The push rods preload the outer cryostat, attaching to the yoke at the outer radius, passing through a radial slot in the yoke to the outer cryostat.

The wrap was tested at 2000 V DC during the wind. Aluminum covers were added after the coil was wound, and the entire assembly heated to 125 °C to cure the epoxy. See Fig. 9.8.

The outer coil contains two penetrations, one to permit the beam to enter the ring, and one which could have permitted high voltage to be fed to a proposed electrostatic muon kicker. It was decided at the time to make this “kicker penetration” in the outer coil, but not to make a hole through the magnet yoke until it was shown that this kicker could be built (which was not demonstrated).

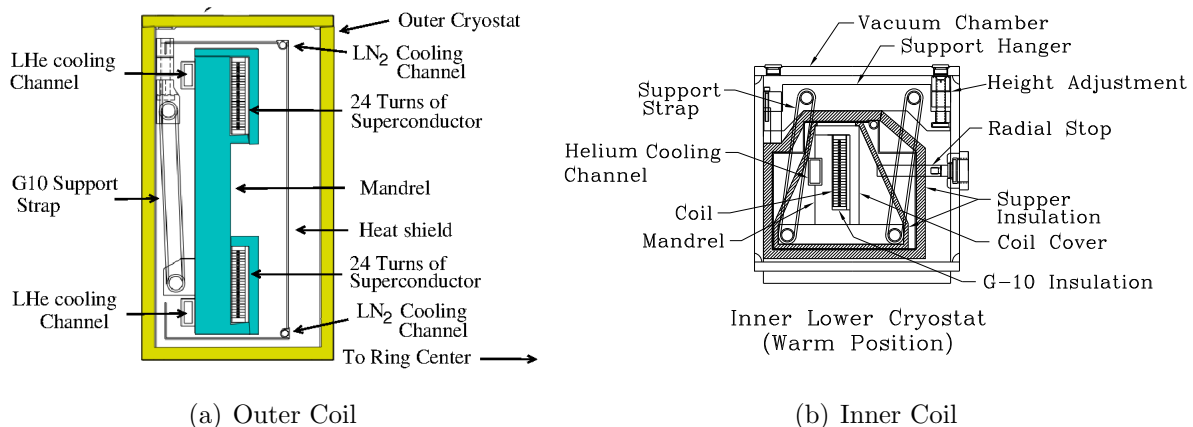


Figure 9.8: The outer and inner coil structures. Both are shown in their warm configuration.

The coils are indirectly cooled with two-phase He flowing through channels attached to the mandrel, as shown in Fig. 9.8. The two-phase helium cooling avoids the increase in temperature that would occur in a circuit cooled with single-phase helium. The operating

Table 9.2: Superconductor parameters

| | |
|----------------------------|------------------------|
| Superconductor type | NbTi/Cu |
| Nominal dimensions | 1.8 mm \times 3.3 mm |
| NbTi/Cu ratio | 1:1 |
| Filament 50 μ m | |
| Number of filaments | 1400 |
| Twist pitch | 27 mm |
| Aluminum stabilizer type | Al extrusion |
| Ni/Ti composite dimensions | 3.6 mm \times 18 mm |
| Al/(NbTi + Cu) ratio | 10 |
| RRR (Al) | 2000-2500 |
| RRR (Cu) | 120-140 |
| I_c | 8100 A (2.7 T, 4.2 K) |

temperature of the coils is within 0.2 K of the coldest temperature in the cooling circuit. The advantages of two-phase cooling are: (1) the helium flows in well-defined flow circuits; (2) the total amount of helium that can be flashed off during a quench is limited to the mass of helium in the magnet cooling tubes; and (3) the location of the helium input and output from the cryostat and the location and orientation of the gas cooled leads are not affected by the cooling system [8].

The key to the operation of a two-phase helium cooling circuit is a helium dewar (the control dewar) that contains a heat exchanger. This heat exchanger sub-cools the helium from the J-T circuit before it enters the magnet cooling circuits. This isobaric cooling provides a higher ratio of liquid to gas with a higher pressure and lower temperature than the refrigerator J-T circuit alone would provide. This feature is important for the long cooling channels in the magnet cooling circuits. The use of a heat exchanger in the control dewar reduces the helium flow circuit pressure drop by a factor of two or more. The control dewar and heat exchanger also have the effect of damping out the oscillations often found in two-phase flow circuits. The helium in the control dewar acts as a buffer providing additional cooling during times when the heat load exceeds the capacity of the refrigerator.

The ($g-2$) cooling system was originally designed to have three separate cooling circuits: a 218 m long cooling circuit that cools all three mandrels in series, the lead and coil interconnect circuits that are 32 m long (the gas-cooled leads are fed off of this circuit), and a 14 m long cooling circuit for the inflector magnet. Later the cooling system was modified to permit each of the mandrels to be cooled separately. Ultimately, the ($g-2$) cooling system operates with parallel cooling circuits for the coils, inflector, and lead cooling. Electrically, the three coils are connected in series so that the two inner coils are in opposition to the outer coil to produce a dipole field between the inner and outer coils. The magnet is powered through a pair of tubular gas-cooled leads developed for this application. Each lead consists of a bundle of five tubes. Each tube in the bundle consists of three nested copper tubes with helium flow between the tubes. The copper tubes used in the leads are made from an alloy with a residual resistance ratio of about 64. The lead length is 500 mm. A typical cool down

from 300 to 4.9 K takes about 10 days. Once the control dewar starts to accumulate liquid helium, it takes another day to fill the 1000 l dewar. In operation, the pressure drop across the magnet system is about 0.02 MPa (3.0 psi). We initiated several test quenches and had one unintentional quench when the cooling water was shut off to the compressors. The peak measured pressure during a 5200 A quench was 0.82 MPa (105 psi). Other places in the cooling circuit could have a pressure that is 40% higher. The quench pressure peak occurs 11 s after the start of the quench. The quench pressure pulse is about 12 s long compared to current discharge time constant at 5200 A of 31 s. The outer coil mandrel temperature reaches 38 K after the quench is over. Re-cooling of the magnet can commence within 5 min of the start of the quench. After a full current quench, it takes about 2 hours for the outer coil to become completely superconducting. The inner coils recover more quickly.

Table 9.3: Estimates of cryogenic heat leaks

| | | 4.9 K load (W) | 80 K load (W) |
|-------------------------|------------------------------|-------------------|------------------|
| Magnet system heat load | Outer coil cryostat | 52 | 72 |
| | Two inner coils | 108 | 77 |
| | Inflector | 8 | 5 |
| | Interconnects | 11 | 46 |
| | Magnet subtotal | 179 | 200 |
| Distribution | Helium piping | 19 | |
| | Control dewar | 5 | |
| | Interconnects/valves | 33 | 32 |
| | Nitrogen piping | | 34 |
| | Distribution subtotal | 57 | 66 |
| Lead gas (1.1 g/s) | Equivalent refrigeration | 114 | |
| Total refrigeration | | 351 | 266 |
| Contingency | | 70 | 51 |
| Cryogenic design | Operating point | 421 | 308 |

Both persistent mode and power supply excitation were considered. The total flux, $\int \vec{B} \cdot d\vec{s}$, is conserved in persistent mode. However, room temperature changes would result in changes in the effective area. Thus although the flux, is conserved, the magnetic field in the muon storage region is not. Persistent mode would also require a high-current superconducting switch. Power supply excitation with NMR feedback was chosen, although no feedback was used for the 1997 run. This method gives excellent control of the magnetic field and allows the magnet to be turned off and on easily. The power supply parameters are shown in Table 9.5.1.

The quench protection design parameters were determined by the requirements of magnetic field stability and protection of the magnet system in case of a quench. When the energy is extracted, eddy currents are set up in the iron which oppose the collapse of the field. This can cause a permanent change in the magnetic field distribution [9]. This is sometimes called the ‘umbrella effect, since the shape of the change over a pole resembles an

Table 9.4: Power supply parameters

| | | |
|---------------|--|---|
| Rating | 5 V, 6500 A | |
| Rectifier | 480 VAC input, 12 pulse (Two $\pm 15^\circ$, 6 pulse units in parallel) | |
| Output filter | 0.4 F | |
| Regulator | Low-level system | 0.1 ppm stability with 17 bit resolution |
| | Power section | Series regulator with 504 pass transistors |
| Cooling | Closed loop water system with temperature regulation | |
| Regulation | Current-internal DCCT | ± 0.3 ppm over minutes to several hours |
| | Field-NMR feedback (current vernier) | ± 0.1 ppm (limited by the electronics noise floor) |
| Manufacturer | Bruker, Germany | |

umbrella. The eddy currents are minimized if the energy is extracted slowly. There will also be eddy currents in the aluminum mandrels supporting the coils. Electrically, this can be represented by a one turn shorted transformer. These eddy currents will heat the mandrels and can cause the entire coil to become normal. This is called quench-back. This has several beneficial effects. The part of the stored energy that is deposited in the coil is deposited uniformly over the entire coil and mandrel assembly. Also, once quench-back occurs, the energy extraction process is dominated by the quenchback and not by the specifics of where the quench occurred. Therefore, the effects of a quench on the reproducibility of the magnetic field should be minimal.

The energy extraction system consists of a switch, resistor, and quench detection electronics. An energy extraction resistor of $8 \text{ m}\Omega$ was chosen. Including the resistor leads, the room temperature resistance is $8.8 \text{ m}\Omega$. This gives an $1/RC$ time constant of 1 minute. The actual time constant varies due to the temperature increase of the coil and dump resistor and the effect of eddy currents in the mandrels during the energy extraction (see below). This resistance value was calculated to cause quenchback in the outer mandrel within 2 seconds at full current. The quench protection circuit for E821 is shown in Figure 9.9.¹ The energy extraction trigger for a quench which originates in one of the coils is the voltage difference between matching coils; for example, $V(\text{outer} - \text{upper}) - V(\text{outer} - \text{lower})$. Since the inductance is effectively the same, the voltages should be equal even while charging the magnet, unless a quench develops in one coil. This quench threshold is set at 0.1 V. However, the coil interconnects are thermally coupled together with the helium tubes. It is possible that a quench in an interconnect could propagate to both coils almost simultaneously. Therefore,

¹These items are at the end of service life. The replacement system is described below.

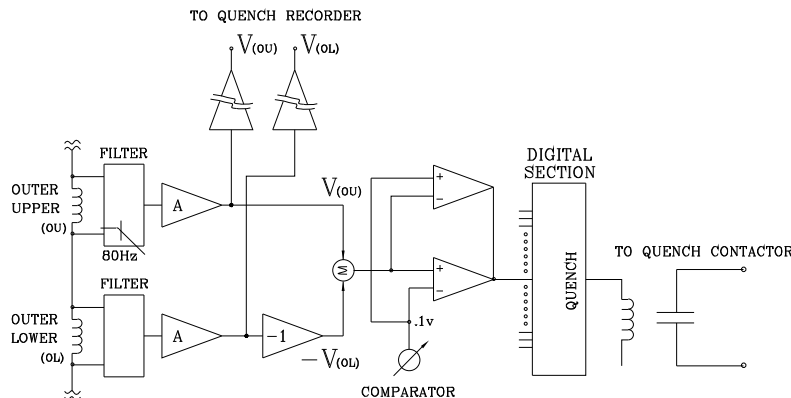


Figure 9.9: Diagram of the quench protection circuit for E821.

a voltage threshold of 10 mV was chosen for each interconnect. The outer upper to lower interconnect is only 1 m long. This threshold was set to 5 mV. The thresholds were determined by the requirement that the quench be detected within 0.2 s. The gas-cooled leads develop a voltage of typically 15 mV at full current. If the lead voltage exceeds 30 mV, the energy is extracted.

9.5.2 Preparations Prior to Transportation

No significant changes will be made to the design, and nearly all components are reused from E821. The WBS sections below describe the steps to reassemble and recommission the items above. We will not need to fabricate any parts, other than to replace old components or to build spares.

Prior to the coil transportation, room temperature tests were performed to verify as much as possible the working state of the system. These were:

- Electrical verification of the instruments connected to the coil and/or mandrel. These refer to the temperature probes, voltage taps for quench detection, and strain gauges. The instruments connected to the cryostat consists of thermometers, voltage taps, and strain gauges. These are indicated in figures 9.10 and 9.11. The strain gauges are attached to the straps, which counteract the Lorentz forces, and the radial stops, which counteract the shrinking of the radial stops due to cooling.

Outer Cryostat Thermometer and Strain Gauge Locations

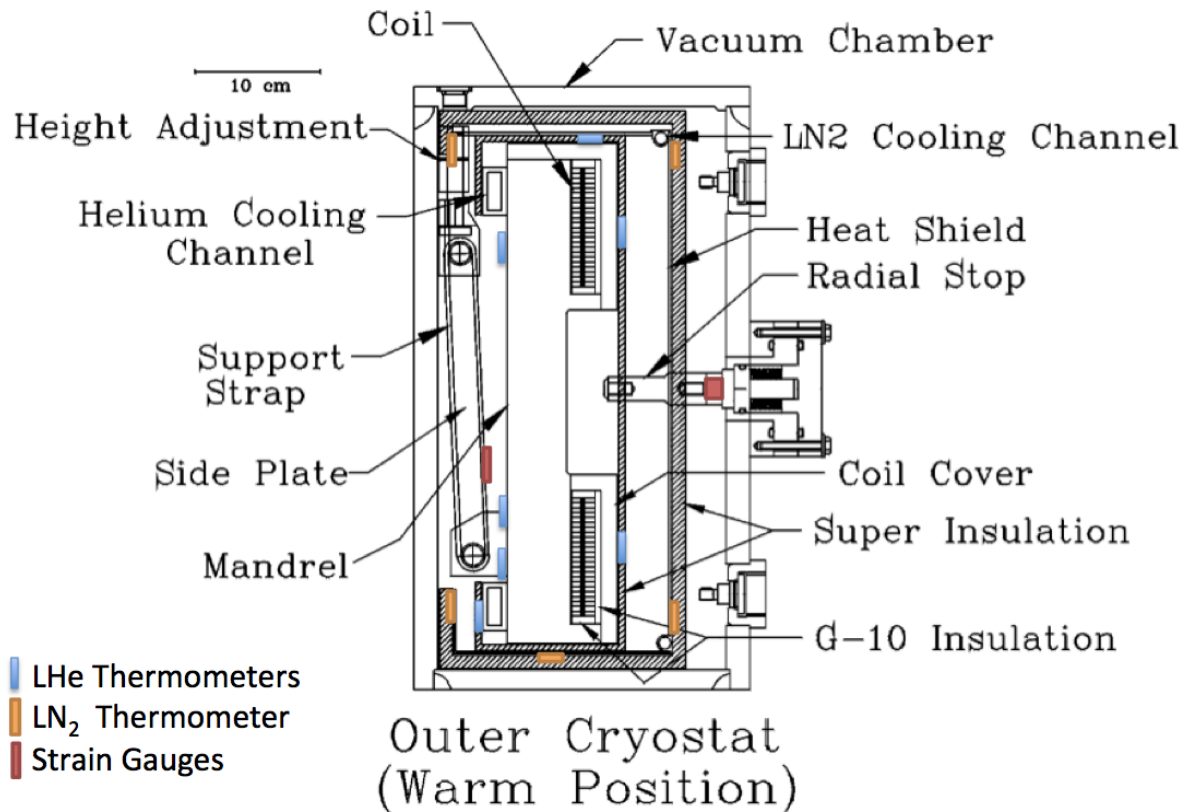


Figure 9.10: Location of outer coil instrumentation, showing the LHe LN₂ thermometers, and strain gauges. There are typically eight thermometers placed at each azimuthal location, with the positions indicated above.

- Resistance measurements of the coil at room temperature, which agree with measurements performed in 1995 (see table 9.5).
- The resistance between the coil leads and ground was measured to be a few kohms, where as an open resistance was expected. Further tests showed the 'short-to-ground' occurring at the connection between the inner lower coil and the power supply (see figure 9.16), and is a straight-forward repair. There is no short within the coils themselves. This short was likely present during E821 running, and would have contributed a 0.01 mA current-to-ground, out of a total of 5200 A. This is 2 ppb effect and would not have been seen in E821 (see references [11] and [12]).

Following this verification, the interconnections between the three coils (see figure 9.12) were separated by a grinding wheel. The temperature was monitored and kept well below 100 °C during the process to minimize degradation to the Aluminum resistance and the NbTi current-carrying capacity. Figures 9.13 and 9.14 show the details of the welds that were cut in this region.

Inner Cryostat Thermometer and Strain Gauge Locations

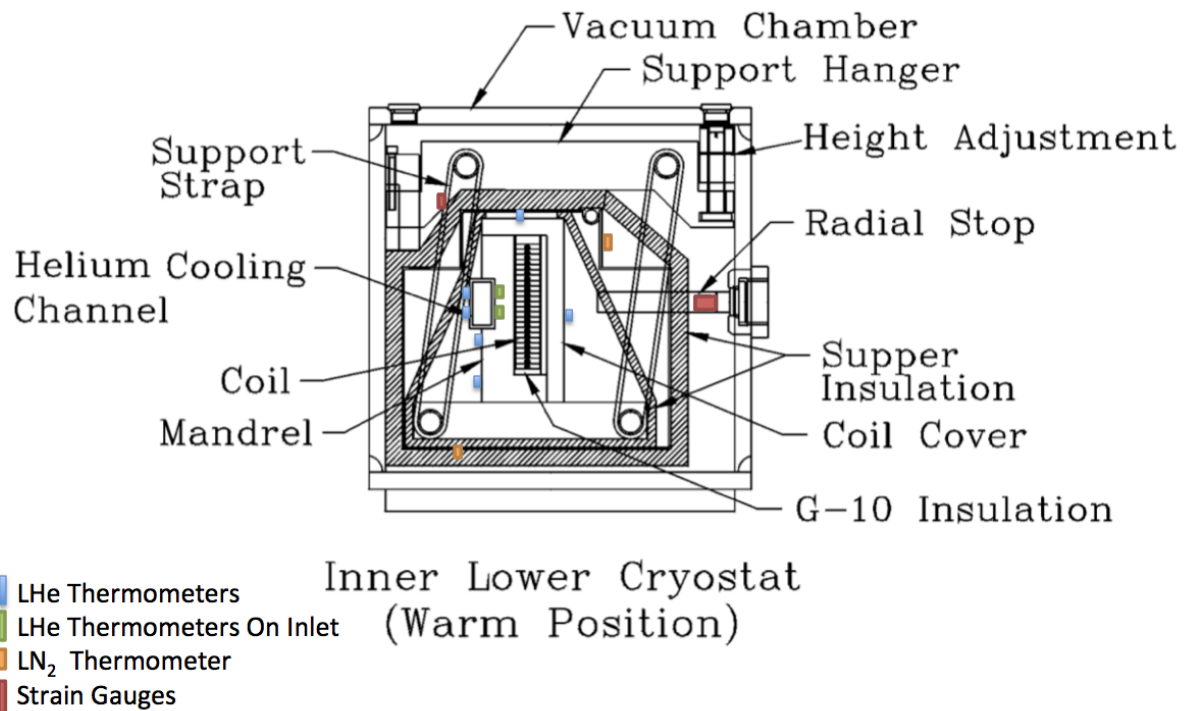


Figure 9.11: Location of the lower inner coil instrumentation, showing the LHe and LN₂ thermometers, and strain gauges. The instrument locations are symmetrically placed for the upper coil instruments. There are typically eight thermometers placed at each azimuthal location, with the positions indicated above.

9.5.3 Cryostat Vacuum Chambers

This WBS consists of the vacuum chambers that provide the thermal insulation for the coils. After the interconnects have been rewelded (see section 9.5.9), the vacuum flanges enclosing that region will be reconnected.

For transportation, a vacuum port connected to the outer cryostat was cut in order to gain clearance. Therefore, this pipe will be rewelded upon reassembly at Fermilab.

9.5.4 Vacuum Pumps

New or refurbished ‘dry’ vacuum pumps will be used to pump down the cryostat vacuum chambers. The pumps must remain a few meters away from the storage beam region in order to not perturb the precision magnetic field. The vacuum quality needed is about 10^{-4} Torr.

E821 implemented a mechanism described below to deal with a potential failure mode called the “cold cryostat problem”. In the event of loss of cryostat vacuum while the coils are cold, the cryostat walls will also become cold and therefore will shrink. Such could happen

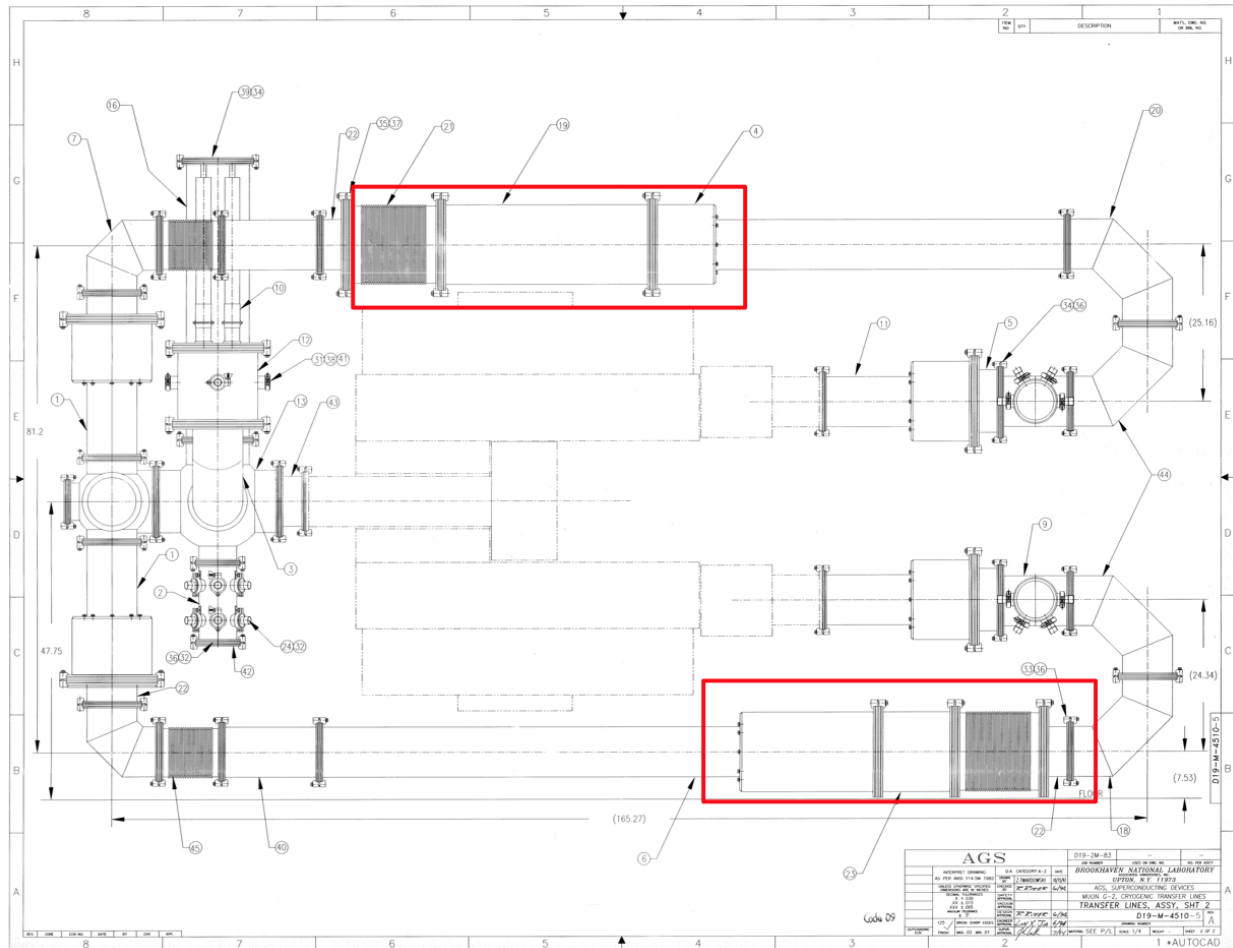


Figure 9.12: The connections between the three coils are indicated. The upper(lower) red box is the connection between the outer-upper (outer-lower) coil and the inner-upper (inner-lower) coil.

if the cryogenic lines leaked cryogenics into the vacuum. The outer cryostat will shrink until it hits the pole pieces. Therefore, the cryostat wall could experience stresses exceeding the allowable value for Aluminum.

For this potential failure scenario, E821 implemented a scheme to trigger a large Roots blower vacuum pump to rapidly evacuate the vacuum chamber.

9.5.5 Power Supply and Quench Protection

The power supply, a Bruker type B-MN5/6500 linear supply, for the main ring will be the same unit used in Brookhaven and as described in reference [3]. Therefore, the design and specifications, and regulation mechanisms for operation will also be the same. The power supply and quench protection cabinet was moved from Brookhaven to Fermilab in mid-November of 2013, specifically to the Dzero Assembly Building (DAB) pit.

Various aspects of the Bruker supply, the quench protection cabinet, and quench detection electronics have been reexamined and recommissioned at Fermilab DAB. The findings are

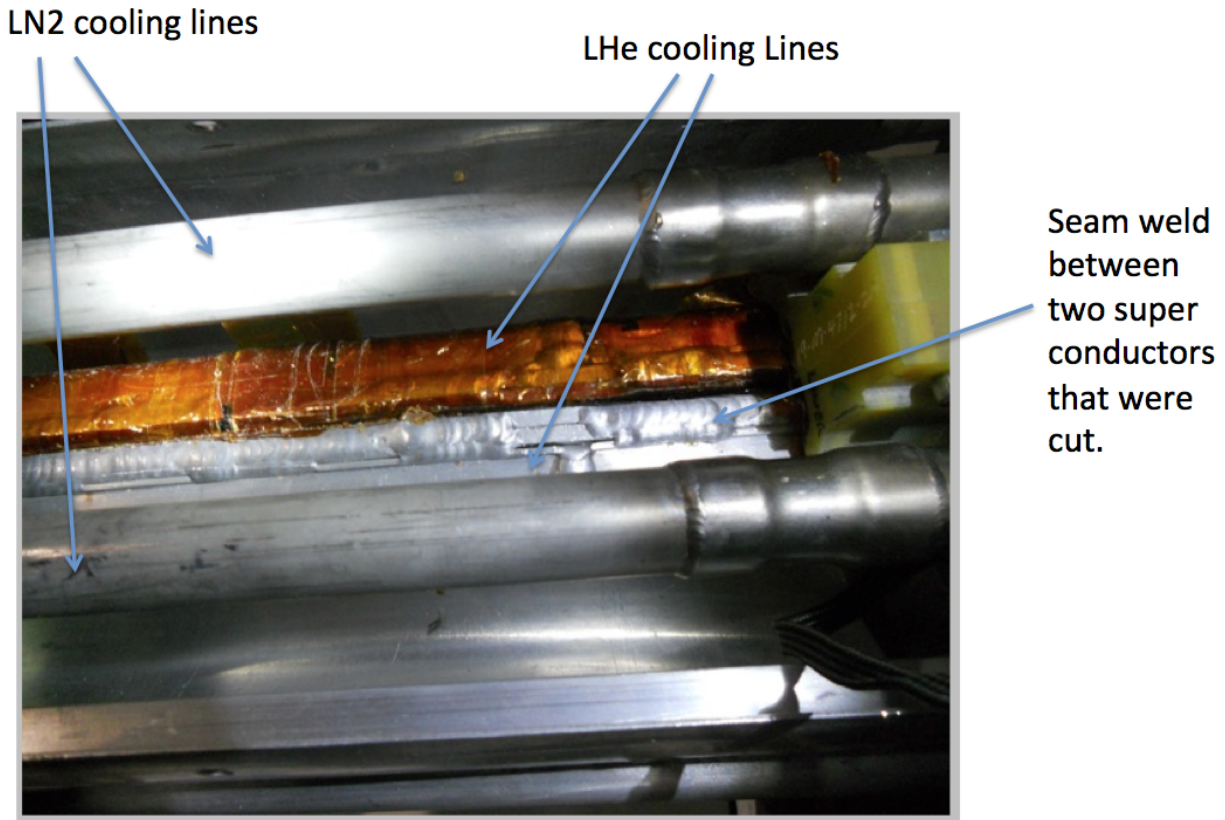


Figure 9.13: Photograph of the region of the interconnection, indicating welds and cooling lines.

described in reference [37].

Power Supply Refurbishment and Modifications

Based on the findings, there are four areas of the Bruker power supplies implementation that needs to be modified or upgraded: cooling, controls, pass bank monitoring, and repair or replacement during operation. Overall, the assembly of the Bruker components within the cabinet is quite integrated inside of a relatively small cabinet space. This means that to get to a series of components, a major disassembly process will be required. Therefore, disassembly, where it is not absolutely required, shall be kept to a minimum. However, the following tasks should be implemented:

- **Cooling:** The cooling supply and the return for the Bruker cannot be directly connected to the chilled water supply system due to the relatively low maximum operating pressure of 8 bar (about 120 psi) and the large cooling flow requirement of 70 Liters/minute. In addition, the cooler the electronic components can be kept during operation, the better given the age of these components. Therefore, a separate regulated cooling system, as described in reference [33], will be implemented.

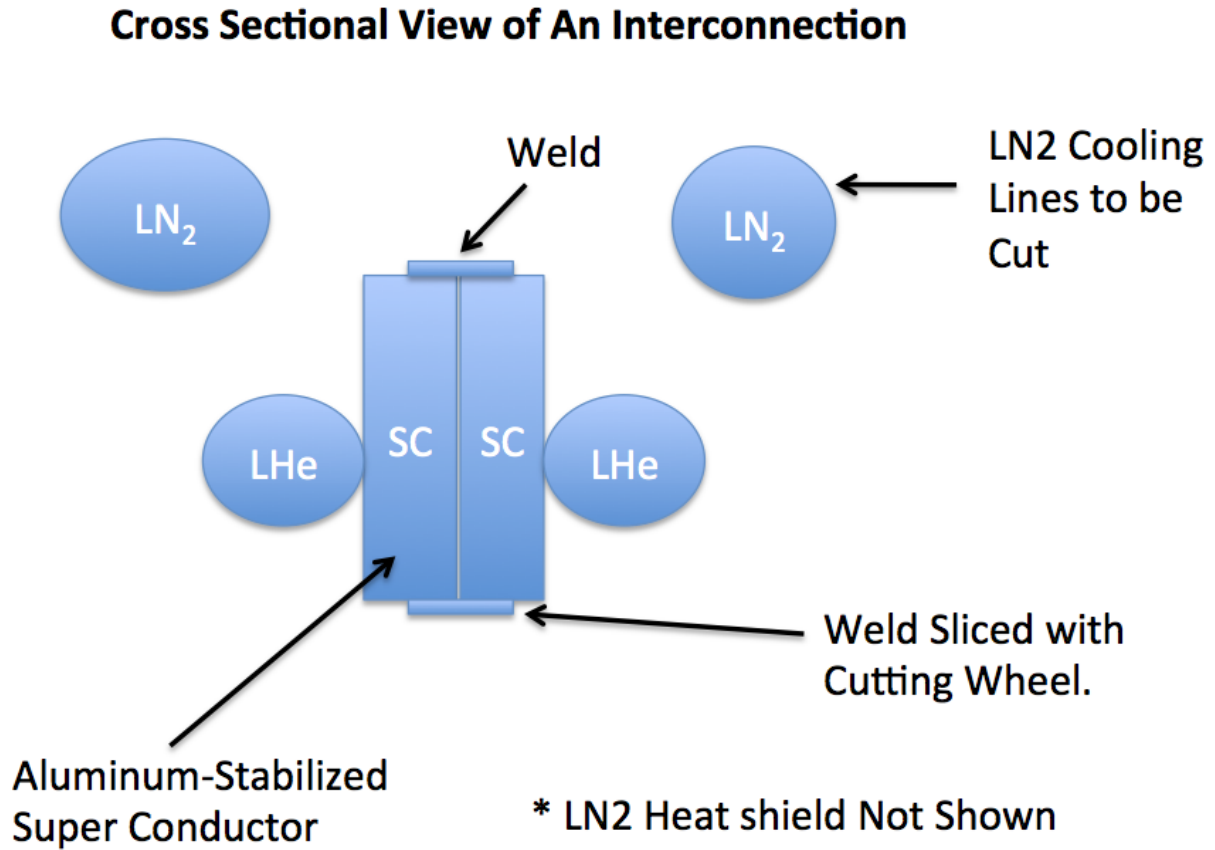


Figure 9.14: Diagram of the region of the interconnection, indicating welds and cooling lines that were cut, in order to facilitate the transportation.

- **Controls:** The original controls for the Bruker uses RS232 command words as described in reference [34] for remote control of the power supply. Local/remote control is implemented using a keyed selector switch. Therefore, it does not appear that front panel operation and remote control can occur at the same time. To implement the control and operation of the Bruker within the Muon g-2 control system, the RS232 interface must be connected to an emulator, either using LabView or a Beckhoff controls unit that can be accessed using Ethernet.
- **Pass Bank:** The output current is a summation of the outputs of 28 pass bank circuits, each containing 18 power transistors. As examined, there is no protection or monitoring of each pass bank to indicate a failed pass bank. Therefore, if one pass bank should fail, the current requirements for the other remaining ones increase. This could lead to a zipper-effect failure that can occur rather rapidly and thus take out the entire supply. Some sort of monitoring will be required on each pass bank to detect a failure and thus to shut down the power supply before this zipper effect can occur.
- **Repair:** As stated, replacement of a pass bank, or the transistors within a pass bank, will not be an easy undertaking and therefore, downtime can be problematic. In

| Coil | Resistance (ohms) Sept-1995 | Resistance (ohms) Dec-2011 |
|---------------------|-----------------------------|----------------------------|
| Inner Upper | 0.429 | 0.430 |
| Inner Lower | 0.426 | 0.430 |
| Outer Upper | - | 0.483 |
| Outer Lower | - | 0.476 |
| Outer Upper + Lower | 0.952 | 0.958 |

Table 9.5: Room temperature coil resistance (ohms) measurements, showing consistency between Sept-1995 and Dec-2011.

addition, there are no spare parts that came with the Bruker. To reduce downtime in the event of a pass bank failure, several spare pass banks (10% or three units) should be fabricated and the transistors matched to the existing pass banks characteristics. Other components, for which spares should be available, will be identified. These include the controls power supplies and printed circuit board components.

9.5.6 Quench Protection System

For the Main Ring, a quench protection system is illustrated in the simplified diagram below (see figure 9.15). This differs with the diagram from the conceptual design report in some important aspects. First, the trip cabinet employs just a SPST DC breaker. It is not a selector switch. Once a quench is detected, the DC breaker disconnects one power supply output lead from the Main Ring lead.

Second, the blocking diode, located in the trip cabinet, conducts only during a quench due to the reverse direction of the quench current from the collapsing field and this current is then dissipated in the dump resistor. Thus, the end result of the quench detection system is a signal that trips the DC breaker. As shown, this signal is generated by any one of four conditions: an interlocks drop or some safety condition, one or more of the threshold levels are exceeded, an intentional trip due to the active pressing of one or more of the crash switches, or the failure of the main power supply.

9.5.7 Quench Protection Circuitry

As the E821 quench protection electronics have reached the end-of-service life, we will adopt the system that was used for the Dzero Solenoid quench protection [32]. The Dzero system is available for E989 use, and has the ability (without redundancy) to serve both the Main Ring and Inflector magnets. In case there is insufficient channel count, a second (backup) option is to construct a LabView based system similar to that used at Fermilabs superconducting magnet test facility, as described in reference [36]. Whichever specific system is used, figure 9.16 illustrates the overall circuitry to be implemented. The voltage thresholds for the generation of a quench trip signal will be set to the levels as used in the Brookhaven system for E821 and as described in reference [3].

- Coil Voltage: 100 mV

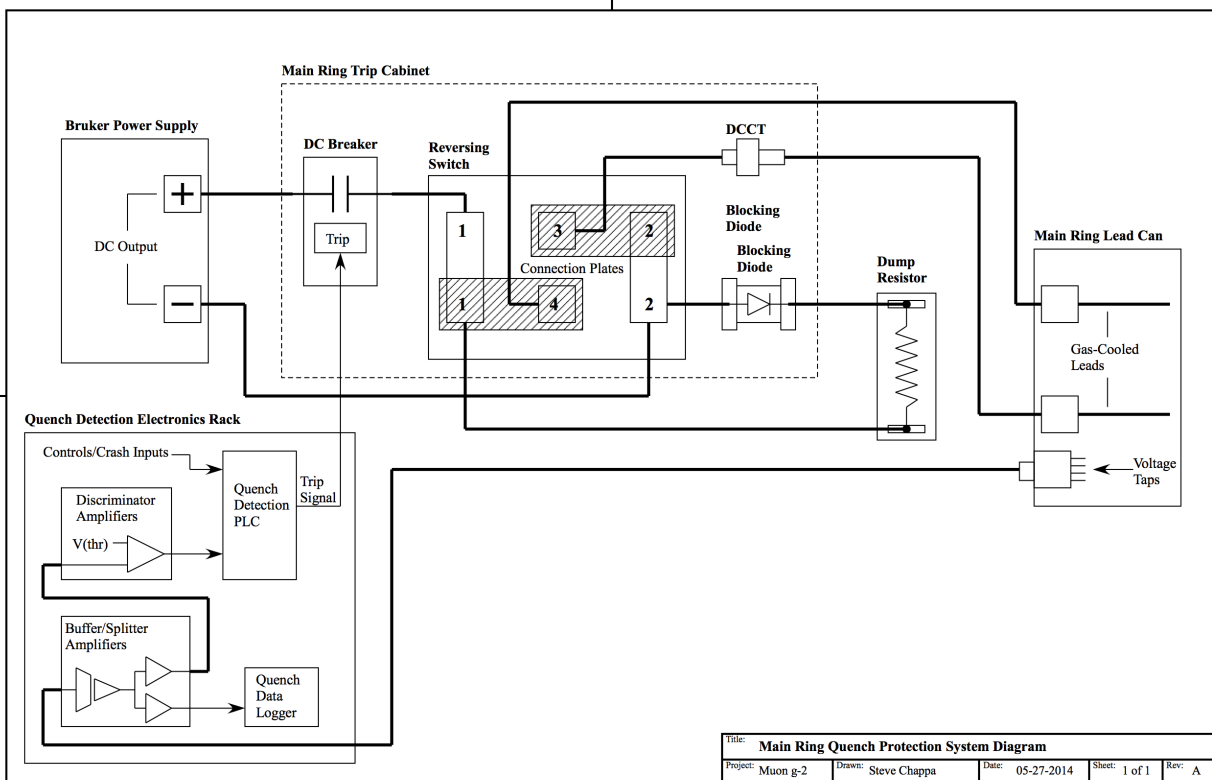


Figure 9.15: The Quench Protection System Diagram.

- Gas-cooled lead: 30 mV
- Outer/Inner coil interconnects: 10 mV
- Upper/Lower coil interconnects: 5 mV

In order to document the specific wiring and connector information of the Main Ring, a wiring schematic is being developed. According to the information at present, a draft of this schematic is shown in reference [35]. Once verified, this schematic will be used to diagram the specific voltage taps to the connectors.

Power Supply and Quench Component Placement

As of now, the plan is to locate the Main Ring power supply and quench protection components within the main hall in MC-1 in a similar manner to that used in E821. The exact location on or near the platform will depend on the exact space and orientation of the components (trip cabinet, quench protection, electronics rack, etc.). The dump resistor will be placed outside of the main hall so as to not adversely affect the temperature within the hall. For runs of the DC output bus that exceed 10 or so feet, water-cooled 10KA bus work can be implemented to save on cost associated with the use of 535 cm locomotive cable.

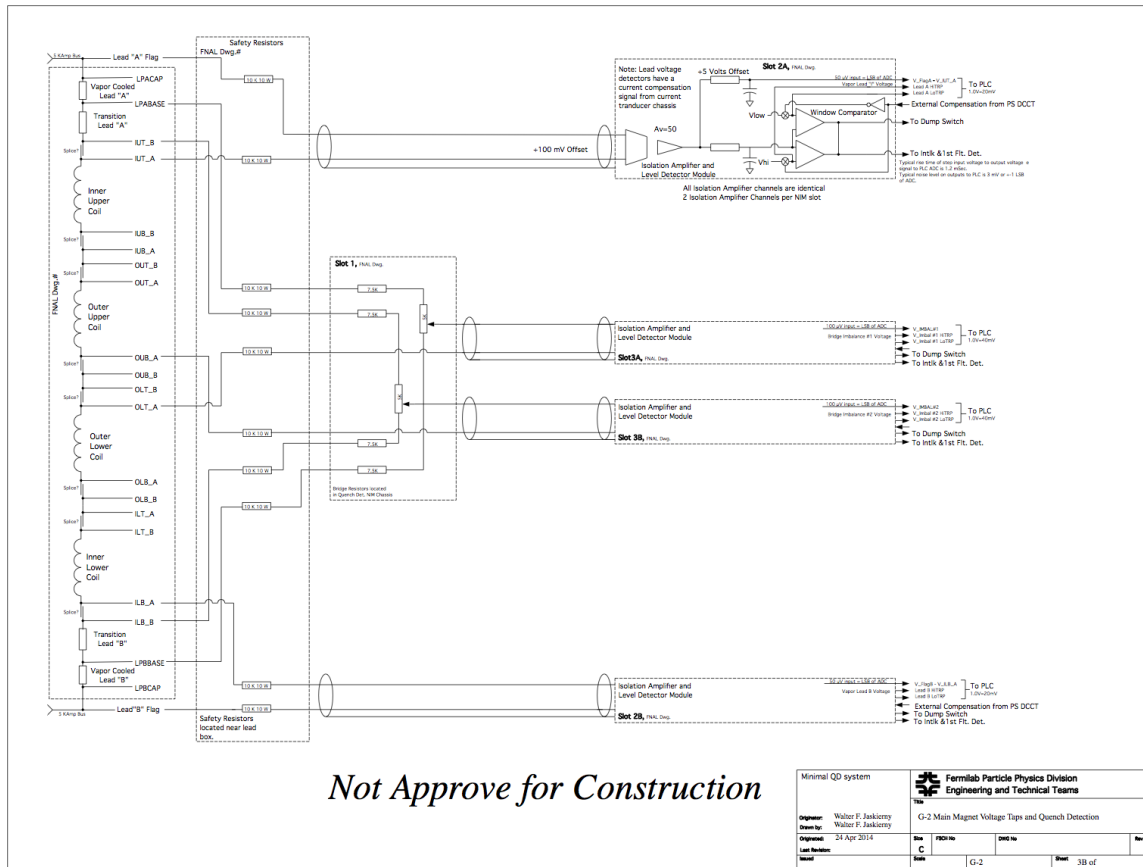


Figure 9.16: Main Magnet Voltage Tap and The Quench Protection System Diagram.

9.5.8 Cryogenics

This WBS refers to the cryogenics (LHe and LN₂) required to cool the coils to 4.9 K, the cooling lines, the heat shields cooled to LN₂ temperatures, and the flow control valves. The E821 cryosystem will be reused as much as possible, especially the 1000 liter dewar. The E821 cryogenic flow diagram is shown in figure 9.17.

While no design changes will be made, this WBS requires considerable verification, reanalysis, and documentation due to the significant hazard and stored energy, and the potential for the ‘cold cryostat’ problem as described in the section above.

The documentation were generated for E821, and will be reaccessed for E989. Attention will be given to:

- Heat load of the system. There will be a slight increase due to the rewelding of the coils at the interconnection (see section 9.5.9) and a slightly longer run between the cryogenic plant and the LHe dewar.
- Flow diagram, pressure drops, and flow rates. These are specified to be identical to that of E821.

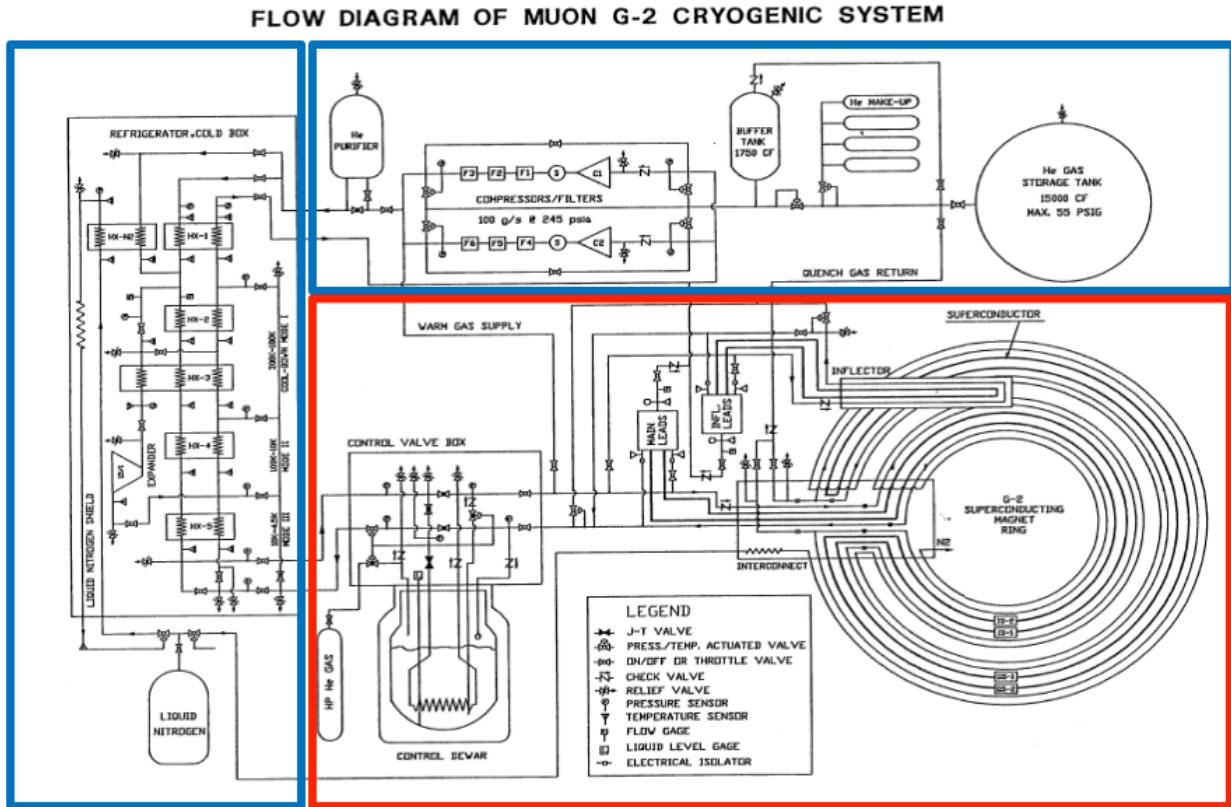


Figure 9.17: The cryogenic plant and its connection with E821 (G-2). The red box outlines the flow within building 919 at BNL. The upper (left) blue box outlines the LHe (LN₂) cryogenic plant.

- Cool-down and warm-up procedure.
- Connection to the Controls and Instrumentation WBS.

The Fermilab Accelerator Division (AD) will provide two dedicated refrigeration systems for E989. An important difference between E821 and E989 is that the latter will share aspects of the cryogenic plant with the Mu2e experiment[13]. Mu2e and g-2 helium gasses are mixed together, and therefore share a common compressor. The AD design includes a cryo adsorber to trap contamination.

9.5.9 Super Conducting Coils

After the steel yoke pieces and coils have been reinstalled into the correct position, the recommissioning activities can begin. The key recommissioning activities for this WBS consists of:

- Performing electrical continuity tests of the instruments such as thermometers and strain gauges.
- Performing electrical continuity tests on the coils. This also verifies unwanted thermal shorts.

- Rewelding the coil interconnects using pure Aluminum filler using the TiG (Tungsten inert Gas) welding technique.
- Rewelding the LHe and LN₂ cooling lines in the interconnection region.

During the interconnect cutting and the TiG rewelding process, a small amount of degradation to the pure Aluminum stabilizer is to be expected due to work hardening. Work hardening will cause a resistance increase of the Aluminum, therefore adding to the heat load at 4.9 K and a small local heating at the interconnection region.

It also reduces the critical current capacity (I_c) before the superconductors become normal. For the welding that took place during the E821 construction, the SC coil heating due to welding was modeled. The maximum temperature seen by the SC coils due to welding is 350°C[3]. Degradation of NbTi critical current of < 5% was measured for a 2 T field for an annealing time of 10s at 400°C[9].

For E821, the coil current and temperature were approximately 5200 A and 4.9 K respectively. The magnetic field at the coil was approximately 2 T. The critical temperature was estimated to be 6.2 K, giving a safety margin of 1.2 K[10]. However, the magnetic field at the interconnect is estimated to be < 1 T, and so the safety margin at the interconnect is even greater.

E821 also welded a test overlap joint, and measured a cold resistance of $16 \cdot 10^{-9} \Omega$ at 2 T. At the current of 5200 A, the heat load is 0.43 Watts at 4.9 K, as compared to the cooling capacity of 351 W at 4.9 K (see table 5 of reference [3]).

In summary, the coils were designed with a rather large safety margin. No quenches were observed to have taken place at the interconnects. To be conservative, we will measure the resistance properties of an overlap weld, cut it and reweld, and remeasure the resistance properties. Finally, work hardening of the Aluminum is strongly anti-correlated with yield strength[14]. Therefore, room temperature tests can be performed to gauge the level of work hardening.

We have studied the process of cutting and rewelding the superconductors. Several samples of 20 cm long overlap joints using g-2 super conductors have been produced, and tested at 4.2K and up to 8000 Amps. The results are described in reference [15]. Two 20 cm long overlap joints, made using ER4043 as the aluminum welding rod² were measured having a 7 nOhm and 10 nOhm joint resistance, respectively. They were cut and then rewelded (again using ER4043). The rewelded joints were remeasured to have a resistance of 21-25 nOhm. Extrapolating to the case of a 1 meter overlap joint, we expect the joint to have a 4-5 nOhm resistance. For the actual rewelding, we will use ER1100³ as the welding rod, which is the purest aluminum available.

9.6 Simulations

The E989 collaboration have developed their own Opera2D and Opera3D models of the magnet, which are useful for understanding:

²A general purpose aluminum welding rod with 4.5% to 6% silicon, and 1145 °F melting temperature.

³An aluminum rod with lowest percentage of alloy agents, and 1215°F melting temperature.

- the large magnetic forces on the pole, yoke, coils, and wedge shims. These magnetic forces are input for calculations of the deflections and stresses [16, 17, 18].
- the transients (eddy) currents from magnet quenching. These currents warm up the cryostats, and cause small voltage differences across the ring [21, 20, 19].
- the dependence of the field quality on alignment mismatches, which are input to the alignment tolerances [22, 23, 24, 25].

The E989 models confirm E821's Opera2D and Poisson calculations. Figure 9.18 and 9.19 show force calculations on poles and coils.

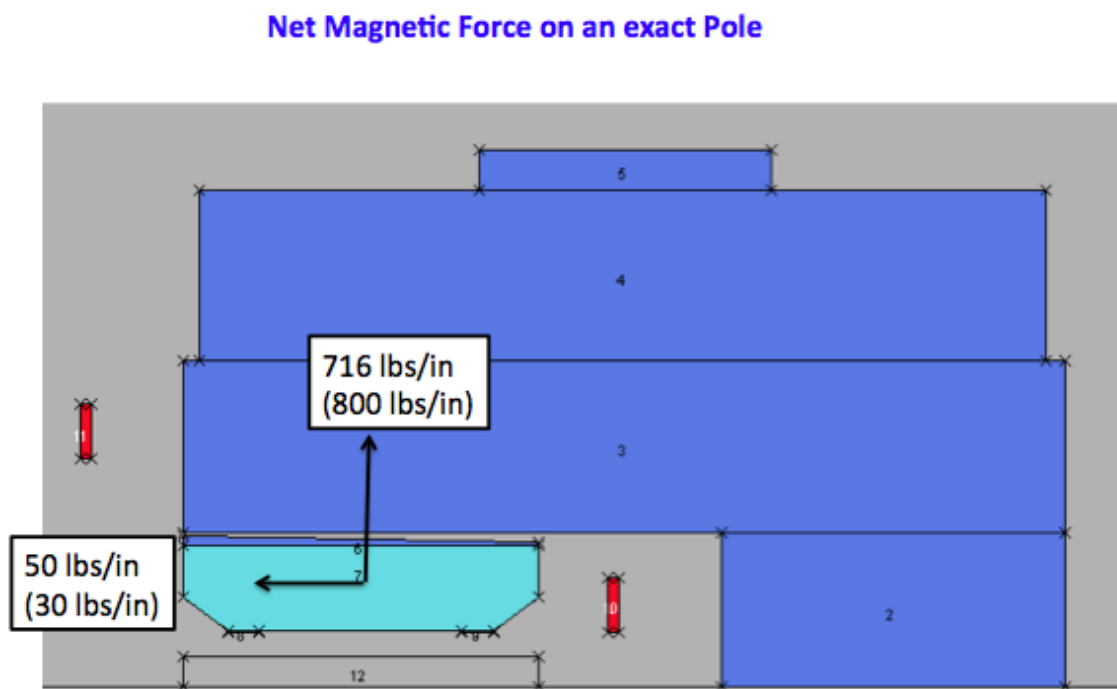


Figure 9.18: Magnetic force on the pole from an Opera2D calculation. The number in parenthesis is a calculation from BNL E821 g-2.

9.7 Alignment

This section of the TDR describes the necessary steps for the alignment of the g-2 magnet ring yokes and poles. Unlike the case of positioning a new accelerator system, this installation requires positioning the components to an existing location derived from BNL E821 measurements. During the construction of the g-2 ring at BNL the designers had the freedom to shape every sixth pole piece to the existing gap. In our case we do not have that degree-of-freedom. So we need to place the components as close to their as-found components as

Lorentz Forces on the Coils

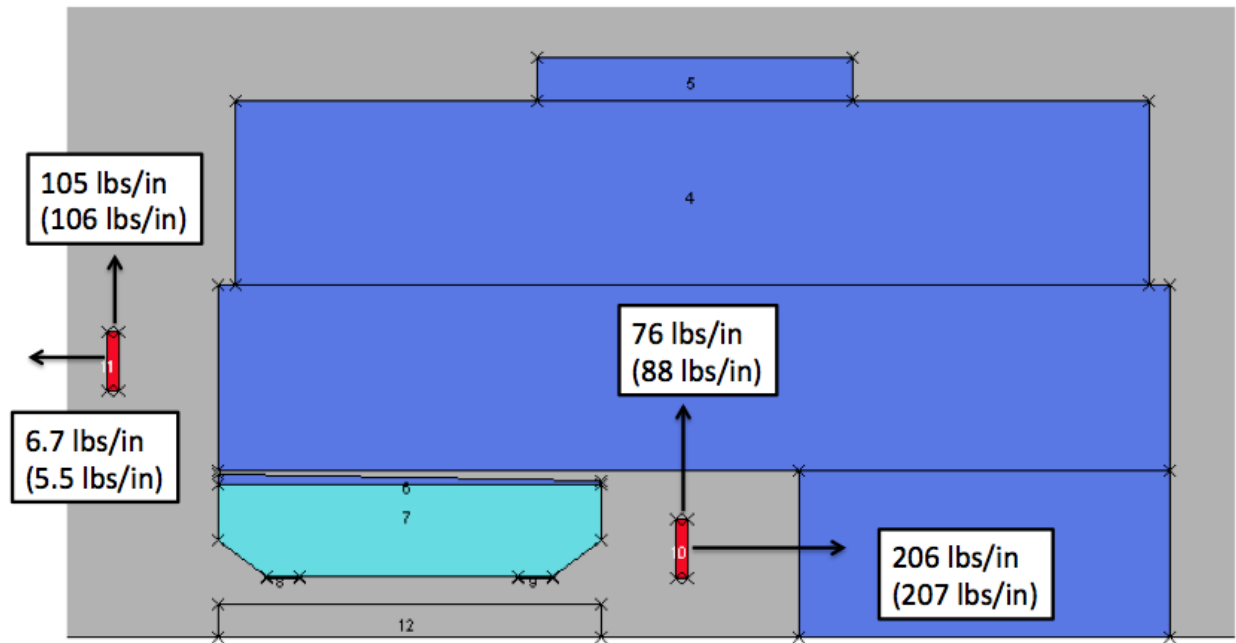


Figure 9.19: Magnetic force on the coils from an Opera2D calculation. The number in parenthesis is a calculation from BNL E821 g-2.

possible in order to close the circle of poles within their tolerances. While we have historical data on these gaps, there is a chance that we need to iterate to the final location in several steps. The following paragraph summarizes the required tolerances.

9.7.1 Required Position Tolerances

For E989, we aim for the tolerance achieved by E821. We fiducialized a subset of the yokes and poles, to verify whether they match the engineering drawings. The following paragraph summarizes the relevant alignment tolerances, and our QC results [26].

Yokes

The machining tolerances for the gap-facing surfaces of the upper and lower yokes were specified to be flat within ± 0.13 mm, and this was confirmed by our QC check of two lower yokes. Both yokes show an RMS of ± 0.03 mm with a peak to peak amplitude of ± 0.1 mm. Similarly, the inner radial tolerance of all yoke pieces is specified to be ± 0.13 mm. Again our QC measurements for two lower yokes confirm that these tolerances have been met for a best fit cylinder radius. However, the radii derived from these measurements deviate by ± 2.5 mm on average from the design radius.

The parallelism for the top and bottom surfaces of the middle yoke (a.k.a. backleg) are specified with an RMS value of ± 0.2 mm, and the thickness tolerance for these parts is ± 0.13 mm. Considering the QC results for the lower yokes, these values will be accepted as face

values without performing QC measurements. The yoke end faces need to be perpendicular to the gap facing surface to ± 0.3 mrad and ± 0.2 mrad in the radial direction. Both of these requirements have been met according to our QC measurements. Similarly, the chord length at the inner and outer yoke radii intersecting the end planes have been machined with an RMS of ± 0.25 mm. Here too our QC measurements confirm this machining tolerance.

The design azimuthal gap between individual yokes was specified to be 0.5 mm. The average reported gap spacing for the inner and outer yoke gaps is 0.8 mm with an RMS of ± 0.2 mm. The lower, middle and upper yokes were matched to equalize the effective azimuthal gap for the three pieces. In the re-assembly this will automatically be achieved as we intend to use the same pieces at the same location as in the BNL setup and the provided pins provide the alignment of these pieces to each other.

Poles

The machining tolerances for the flatness of the pole top surfaces creating the gap between the upper and lower poles were specified to be $\pm 25 \mu\text{m}$ with a ground surface finish of $\pm 0.8 \mu\text{m}$. Errors in pole thickness are small compared to the expected variation in gap distance. QC measurements of 12 poles show a pole thickness variation on the order of $\pm 47 \mu\text{m}$ which only exceeds slightly the manufacturing specification of $\pm 40 \mu\text{m}$.

Naturally, at that level of accuracy any temperature effects need to be taken into account. These effects will play a major role during the re-assembly of the massive steel components of the g-2 magnet ring. Very good temperature stability will be required when we fine tune the position of these components. The machining tolerance for the pole width is specified as $0.56 \text{ m} \pm 50 \mu\text{m}$. The QC measurements of the pole subset show that the average pole width deviates from the nominal value by $20 \mu\text{m}$ with an RMS of $\pm 27 \mu\text{m}$. For the azimuthal pole position, Kapton shims of thickness varying from 40 to $80 \mu\text{m}$ were used. The nominal inner yoke and pole radii are set to 6.83199 m from the ring center. Similarly, the yokes will be placed at that same distance.

Magnet Gap

The nominal gap distance between the lower and upper poles is 180 mm. The gaps between upper and lower poles should be uniform and not tilted when the magnet is energized. Consequently, the upper poles need to be positioned tilted in the radial direction by about $200 \mu\text{rad}$ to account for yoke deformation when the magnet is energized. In other words the gap distance at the inner pole radius needs to be $100 \mu\text{m}$ larger than the nominal gap. Assuming that the lower poles will be set level with respect to gravity at the center of the ring, the upper poles need to be tilted radially to accomplish this requirement. The placement of the gaps in absolute space is less important than the pole-to-pole gap uniformity. No particular value for the absolute placements of the poles has been specified. However, from the historical BNL 821 data, it is obvious that the achieved pole placement stayed within a tolerance band of 0.5 mm while the relative pole to pole positioning achieved an average value of $12 \mu\text{m}$ with an RMS of $\pm 50 \mu\text{m}$.

9.7.2 Superconducting Coils

The superconducting coils operate at 5200 Amps producing a magnetic field of 1.45 T. There are two inner coils, supported by the upper and lower yokes respectively. The third, outer coil, resides inside the C-magnet close to the vacuum chamber. When cooled down to 5°K, the required coil radial position repeatability is ± 0.5 mm, in order to maintain the required field quality. In the cool down process all coils shrink radially by 30 mm while the outer coil expands by 3 mm once powered. The outer coil hangs from the cryostat supported by low thermal-conductivity straps that take up the dynamic changes of the coil during the temperature cycling. The coils are located using radial stops on the inner most radius. For the outer coil the stops transfer the force from the coil to the cryostat box, and push rods from the iron yoke transfer the force from the box to the iron. For the inner coils, pins replace the pushrod. The outer coil is supported at 16 azimuthal locations. Due to the shrinking of the coils when cooled, the outer coil rises by 3.3 mm and needs to be positioned 1.5 mm below the magnet mid-plane under powered conditions. Any vertical adjustments are only possible as long as the upper yokes have not been installed. Consequently this sets the installation sequence. For the positioning of the outer coil, eight radial stops and their associated push-rods are utilized, while eight radial stops are used for the inner coils with the inner cryostat boxes locked at four azimuthal locations.

9.7.3 Alignment Concept

Fermilab operates a multitude of accelerators that are monitored utilizing a site wide survey control network. The origin of this network is congruent with the lattice design programs. The major difference between the lattice information provided by the Accelerator Physics Department and the survey control network is the required transformation between the planar rectangular coordinate system of the lattice to a curvilinear geodetic coordinate system that takes the approximate earth curvature into account as most of our survey equipment references to earths gravity. This setup ensures that the transport line feeding into the g-2 ring magnet and the ring structure are properly located to each other. The control network has been established and the 3D coordinates of the control points are known to ± 0.5 mm. Based on this information we provided the layout of the incoming beam line and ring support plates.

Referencing

The re-assembly of the g-2 experiment at FNAL specifies very tight positioning tolerances, requiring the referencing of all lower yoke steel before placement in the ring. This step calls for the permanent installation of four fiducial markers per yoke. Utilizing a laser tracker system all pertinent yoke features required for the placement of the yokes need to be measured. Using this information we can then best fit the placement of the injection yoke on the incoming injection line and the proper ring location using the control network information. Measuring the locations of the connecting surfaces between yokes one can then determine the necessary shim size between yokes according to the provided BNL historic data. The only variable in this case is the measured nominal radius that needs to be held to a tolerance of $\pm 50\mu m$.

Instrumentation

Depending on environmental conditions, the laser tracker system (LTS) [27] provides 3D point accuracies on the order of $\pm 50\mu\text{m}$ in a spherical volume with radius up to 10 m. This system will be used for all referencing and positioning tasks of g-2 components (see figure 9.20).

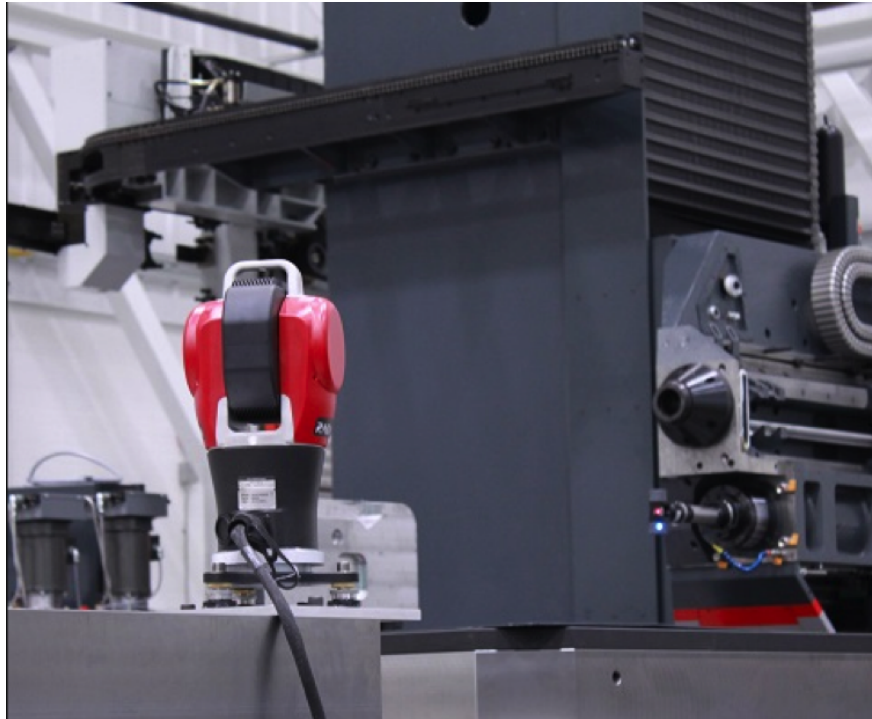


Figure 9.20: The Radian API Laser Tracker System.

Although the LTS is sufficient to provide the demanding position accuracies, it is not capable of fulfilling the elevation requirements. Therefore a separate, ultra-precision HAMAR [27] laser level system will be implemented (see 9.21). Depending on the environmental conditions, this system can provide a level laser plane within $\pm 2.5\mu\text{rad}$ over a distance of 10 m. It is fast and easy to use and will be handy when frequently checking the levelness of the yokes and poles in between installation steps that may affect that dimension. The laser source will be placed close to the center of the ring on a stable Brunson support, while multiple sensors can be used on ring components. In order to capture any drifts or sudden changes in the laser plane three permanent monitoring stations at the ring in-field constantly monitor the level plane and provide information in case the system exceeds the tolerance range. Both of these systems cannot be utilized under operating conditions when the magnet is powered. At that point the BNL shimming trolley will be utilized. This trolley operates without the vacuum chamber installed and features four capacitance sensors at the four corners of the support frame. The Capacitec sensors measure distances to a fraction of a micron over a very limited range and are used to provide the ultimate gap measurement under operating conditions.



Figure 9.21: The HAMAR Ultra Precision L740 leveling laser system.

Position Tools

BNL E821 used primarily the lifting crane, radial adjusters, and jackstand adjustment screws to move the yoke and poles into the final location. For E989, additional tools have been built to adjust the yoke and azimuthal position. A new tool to adjust the elevation of the poles has also been built. These should improve the speed and accuracy of the reassembly.

9.8 Main Ring AC Power and Grounding Plan

The AC power distribution and the grounding for the Main Ring within the MC-1 hall are closely intertwined since the requirements for each function requires the interconnection of components for each system. How these components are connected and where they are connected defines the grounding plan for the main ring and can determine if the system will minimize or propagate noise throughout the ring and its individual detectors. Some of these detectors will require a clean AC power source and a clean and stable grounding system.

9.8.1 Building AC Power Distribution

The AC power within the MC-1 building is divided primarily into four main functions: 1) Building utilities, 2) Accelerator and Beamline power supplies, and 3) Main Ring detector and power supply loads, and 4) Computer and telecomm loads. AC power enters the MC-1 building through two 750 KVA transformers. One of the transformers, 1A, supplies power for the building utilities, the Main Rings clean power, and computer rooms AC power. The other transformer, 1B, supplies power mainly for the Accelerator power supplies and for the Main Ring and Inflector power supplies. Reference [29] illustrates a very simplified and partial Single-Line Electrical Drawing (SLED) that depicts how these circuits are divided up between the two transformers. Reference [28] contains the contractor or construction drawings used to specifically define all aspects of the electrical installation. However, these drawings do not include the distribution circuits used for the Main Ring since these AC power distribution circuits were defined after the MC-1 contracts were issued.

9.8.2 Main Ring and Detector Clean Power

The AC power entering the MC-1 building is usually assumed to meet certain standards as far as distortion from the ideal is concerned. However, there is no set standard to define this distortion in the US. Standards committees, such as IEEE and the IEC, are moving towards developing a universal standard. There already exists a series of guidelines and limitations set forth in several IEEE publications. These standards define limits of any 60 Hz sine-wave deviations such as changes in voltage, frequency, swell, harmonics, etc. If one assumes these standards are met, then the AC power, as seen by the building's feeder transformers, will be pretty much free of these distortions or clean. AC power can be made dirty (distortion) by what the individual loads can put back on the AC line. Thus AC power for certain loads can be kept clean by segmenting them from loads that are known to cause line distortions. Segmenting the loads is done primarily by assigning specific loads to specific distribution transformers. As seen in reference [29], the AC power for the Bruker, for instance, is supplied by a 480 VAC to 480 VAC, delta-to-wye, shielded transformer. This is commonly referred to as transformer isolation. Since only the Bruker power supply is connected to the transformers output, noise and distortion connected upstream on the transformers primary will have little effect on the transformers output and thus the Bruker.

Three other transformers are used in like manner to distribute power to 1) the detector electronic loads, 2) the main ring utilities such as computers and cryo and vacuum pumps, and 3) Main Ring components located outside of the ring such as the Blumlein equipment and various 120/208 VAC outlets. Since each of these transformers are shielded and rated to handle nonlinear loads, such as computers and power supplies, distortion on the secondary of one transformer will not significantly affect the power as seen on the secondary of another transformer. In addition to the separation provided by transformers, there will be transient suppressors installed in each distribution panel to protect the load bus from transients into the panel or transients caused by noisy or faulty loads. Line filtering can also be installed at the load location when incoming power to a piece of equipment or equipment within a rack requires additional protection from AC line noise.

9.8.3 Main Ring Grounding Plan

A grounding plan or strategy is designed to specifically define the interconnections to the earth, AC power distribution, and the MC-1 building. Ground connections are used to perform one or more of the three basic functions: 1) Provide electrical safety ground connections, 2) Provide a low-impedance path for HF noise currents to return to their source, 3) Minimize any voltage potential differences between different metal structures and the earth ground potential and thus minimize ground currents through these metal structures.

Electrical Safety Connections

Connections for electrical safety are governed by the National Electrical Code (NFPA 70) and the provisions and requirements must be followed. If done properly, most, if not all, safety ground connections will have no effect on an electrical systems noise performance.

Low-Impedance Path for HF Currents

HF ground currents, those above 1000 Hz, can be conducted or capacitively coupled between component metal and conductors or can be directly conducted from one metal structure to another. The higher the frequency, the more likely these currents can be coupled. Low-impedance ground connections can provide a path for these currents that is controlled and thus reduce the probability that they will couple into an input to a high-impedance amplifier or some other sensitive circuit component.

Minimize Voltage Potentials

To minimize DC or LF (those below 1000 Hz) currents from flowing through metal structures, grounding connections are specifically made between these structures and to the earth grounding electrode or electrodes. Ideally, the potential between the earth, the building, the electrical distribution, and Main Ring and Detector metal structures would all be zero volts. No potential, no ground currents. However, this is not possible. To implement these connections, two configurations are used: 1) a star or point ground configuration, 2) a grid grounding configuration. Each has their advantages.

9.8.4 Basic Grounding Connection Rules

The basic or fundamental set of rules must accompany a grounding plan. For the Main Ring and MC-1 Hall grounding connections, the following set of rules were chosen:

- Connect the Main Ring metal structures to the MC-1 building structures at one point.
- No floating pieces of metal. All metal or chassis components shall be grounded.
- Follow specific routing of cables along grounded structures. No point-to-point cabling.
- Most cable shield connections are to be made on a case-by-case basis. Generally, shields for cables that exit or enter the Main Ring are connected only at one point or to only one ground structure (coax cables being a special case).

- Avoid the creation of ground loops by adhering rules 3 and 4 listed above.
- Avoid the use of continuous metal or conductors that follow the perimeter of the Main Ring and form a circular path.

Keep in mind that the details of how these rules are implemented and where the grounding connections are made determine how successful the plan can be in creating a low-noise, solidly-referenced grounding environment.

9.8.5 Main Ring Grounding Configuration

The implementation of the Main Ring grounding plan starts with a basic diagram and the connection of four main components: 1) the Main Ring structure, 2) the Main Ring grounding structure arranged in a wheel spoke pattern, 3) the MC-1 building ground structure, and 4) the cable and interconnecting bridge that serves as the start-point grounding connection between the Main Ring and building ground. This star ground configuration prevents building ground currents from being conducted through the Main Rings metal components and ground structure from different sectors of the buildings ground structure. The main disadvantage with this configuration is that effort must be taken to determine and control all connections between the Main Ring and the building.

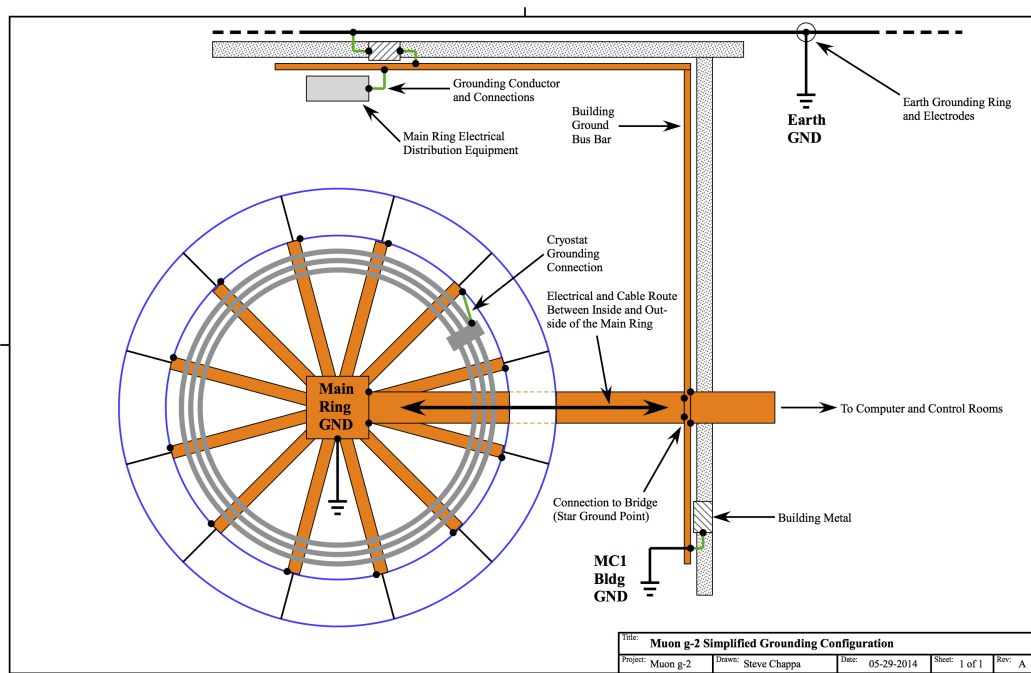


Figure 9.22: A simplified drawing of the grounding configuration. See reference [31] for detailed drawings.

Main Ring Structure

This structure consists of the cryostat rings, the yoke and pole pieces, and ring interconnect. Each of these metal pieces need to be kept at the same potential to limit any current paths between them and to keep the eddy currents minimized by having relatively high-impedance breaks between these yoke sections. Notice that the common connection point for the three cryostat rings is connected to the Main Ring grounding structure only at one point (near the bridge).

Main Ring Grounding Structure

To achieve the grounding connections for the different yoke sectors and for the pole pieces, plus various chassis or metal components on each sector, the grounding path cannot be a circular copper bus as would be easy to implement. Instead, in order to adhere to rule 6, a spoke pattern of flat copper plates (wide copper for HF low-impedance) is used to provide a solid grounding connection for each yoke sector and the metal pole pieces and components within that sector.

Building Grounding Structure

A good building ground structure has all metal parts of that building, the electrical distributions grounding connections, and the earth grounding electrode connections arranged so that there is as much uniformity of ground potential throughout the building. However, this is not the case for the MC-1 hall. The electrical grounding connection to the building is a rather long distance from the area where the Main Rings star ground connection needs to be made. Because of this distance and the limited building connections to the electrical system, additional ground connections between the building and electrical system needs to be made using the wide copper bus bar that runs along the south and west walls (see [31]). This bus also provides a solid, low-impedance grounding connection for the Main Ring. Notice also since most of the cables exiting the Main Ring Needs to go to the computer or the control room, a cable tray with the flat copper plate is used to provide a low-impedance ground connection between the computer and control rooms and the Main Ring star ground point.

Connection Bridge or Star Point

The center part of the spoke grounding pattern is then connected to the MC-1 building ground by the use of a wide copper bridge (wide copper for minimizing impedance at high frequencies). This bridge actually consists of all components necessary for electrical distribution, signal cables, cable tray, and kicker HV coax cables. The reason for this bridge is to provide a controlled path for all cables that connect between the building and Main Ring. By keeping these cable paths next to the common ground structure, this minimizes any cable loop area that might develop between the Main Ring and MC-1 building grounds and thus minimize the likelihood of creating ground loops that can cause noise problems for systems in and outside of the Main Ring.

9.9 ES&H, Quality Assurance, Value Management, Risks

9.9.1 Yoke, Pole, and Shims

The hazards will be in the stored mechanical energy of these very heavy items during the use of the crane during installation. While the magnet is powered, the super bolts will be stressed (stretched) to counteract the magnetic forces' tendency to close the pole gaps. The stored electro-mechanical energy is approximately 6 MJoules. The storage region magnetic field of 1.45T is also a hazard.

Mitigation would be to train the collaboration in proper procedures, controlling access to the area, and implementing a mechanism for detecting high magnetic susceptibility materials so that they are kept away from the high field area.

Quality assurance, value management, and risks concerns are minimal since these items have been built and worked to specifications for E821. They are also passive materials and have high mechanical strength. Since considerable E989 machinery has already developed to model the magnetic field and temperature, we can simulate all alignment requirements.

9.9.2 Power Supply and Quench Protection System

Hazards

The hazards during the testing processes will be primarily electrical. There will be an arc-flash hazard based on the incoming 480 VAC power feed and at 60-amperes. A complete hazard analysis can be made once the units are received and initially examined. The mitigations for these hazards are:

- In the staging area, a safety disconnect switch will be used to provide emergency shut-off of power to the power supply.
- No operation of any component will be done unattended. There will always be 2 persons minimum present during any operation and testing.
- Only properly trained persons, Electrical NFPA-70E and LOTO II at a minimum, will be allowed to work on the equipment.
- Proper PPE and distances will be observed during operation and testing, especially during initial power up and during full-load operation. The level of PPE will be determined once the staging area is set up.

Risks

Risks to the successful completion of the tasks:

- Use of Obsolete Components: Level-Medium. This risk involves the use of relatively old electronics. Therefore, component failure probability (based on hours of previous operation and power cycles, will need to be assessed for critical components of the power supply. Mitigation, at a minimum, will be to list these components and acquire

spares in case of failure. To minimize the effect this risk will have on the schedule, the component list will be generated in parallel with the other operations. Initial costs will be incurred to acquire these spare components.

- **Catastrophic Failure During Testing:** Level-Low to Medium. The units have operated before and they operated as initially designed. Therefore, testing of the components and of the units in stages should provide early indications of failure and allow replacement before the start of connection and commissioning.
- **Difficulty in Acquiring the Proper Testing Equipment:** Level-Low. At this time, most equipment needed for testing, is, or should be, readily available on site. Therefore, purchases of new equipment will be at a minimum.
- **Catastrophic Failure During Commissioning:** Level-Low. The risk here would be the most critical since failure of any component while connected to the ring coils would also present risk to the coils themselves. Mitigation here would be the exhaustive testing of components prior to connection to the ring and the powering up of the ring in stages of load and cooling. In addition, specific procedures for connection to the rings leads will be repeatedly and continuously reviewed.

Quality Assurance

The assurances that the units will operate as required are two-fold: First, the design is already done. Redesign should be at a minimum. Second, there will be exhaustive testing of each component prior to re-assembly. These testing procedures will be continuously reviewed during and after each stage of testing. Again, the primary process for all this is the initial examination followed by testing in stages as opposed to a one-time, massive final test. The staged testing allows deficiencies or problem areas to be identified at the earliest possible point in the task schedule. This again stresses the importance of the initial examination for the results of this will determine, in large part, the testing schedule.

Value Management

As much reuse of components will be implemented throughout these processes. Also, preliminary examination will serve to spot questionable components. Overall, the refurbishment process is used to minimize the need to purchase or redesign components and systems. Since the design is already done and it operated as designed, the risk and extra effort in developing a new design can be kept to a minimum.

9.9.3 The Cryogenic and Related Systems

The hazards are related to the use of LHe and LN₂ cryogenics: thermal energy and ODH. As described above, if the cooling lines in the vacuum cryostat leak, there is potential for the ‘cold-cryostat’ scenario (see above). These can be mitigated in the same fashion as E821. The cooling lines and vacuum chambers can be pressure tested at room temperature, following delivery from BNL and prior to use.

New quality assurance and value management requirements are minimal since these items have been built and worked to specifications for E821. Should the items fail during recommissioning, they can be easily replaced since they are commercially available items of reasonable cost. These are vacuum parts and cryogenic lines. The only outstanding technical skills required are Aluminum welding and vacuum leak-testing.

There are inherent risks in nearly all cryogenic systems since these are usually very complex and have long time scales. Even though E821 operated a successful system, significant engineering is required for recertification. A mitigating factor is that similar systems have been built at Fermilab, and is inline with the expertise of the project mechanical engineer.

9.9.4 The Superconducting Coil System

The coils systems do not present a significant health hazard. Quality assurance and value management concerns are minimal since these items have been built and worked to specifications for E821.

The risks are not considerable. The risk of damage to the coils, straps, heat shields, glue joints are minimal since the stresses expected during transportation are at least 4x smaller than the maximum allowable stress. The expected stresses and deflections due to transportation have been simulated by FEA.

However, we itemize them here since the replacement cost of the coils is beyond the scope of the project:

- The coil windings are on the inside radial surface of the mandrel, rather than on the outside. During power up, the coils push against the mandrel, thereby enhancing the thermal cooling. Therefore, the system can tolerate failures of the glued interface, which is designed to enhance thermal conductivity.
- Failure of the straps, though unexpected, can be detected as we slowly energize the coils. If a strap fails, it can be detected as a shift in the coil vertical position. It can be repaired by cutting an access hole in the vacuum cryostat. The downtime would be of order 2 weeks.
- Failure in the heat shield can be detected as the system taking too long for cool down. Failure of the cooling lines can be detected as loss of vacuum. These are repaired via cutting access holes into the vacuum cryostat. However, it will be difficult to locate the point of failure.
- There is a very slight risk of the Aluminum resistance at the interconnection becoming too high during the reweld. We are currently prototyping the rewelding process and study the correlation of resistance with yield strength. We can anneal the interconnection to improve the resistance.

References

- [1] Bailey J, et al. Nucl. Phys. B150:1 (1979).
- [2] Bennett GW, et al.(The Muon ($g - 2$) Collaboration) Phys. Rev. D, 73:072003 (2006).
- [3] G.T. Danby, et al., Nucl. Inst and Meth. **A 457**, 151 (2001).
- [4] Reference Manual for the POISSON/SUPERFISH group of codes, LANL, LA-UR-87-126.
- [5] Design Report, BNL E821, A New Precision Measurement of the Muon ($g - 2$) Value at the level of 0.35 ppm. 3rd edition, D.H. Brown et al. B.L. Roberts Editor, March 1995.
- [6] A. Yamamoto, H. Inoue, H. Hirabayashi, J. Phys. 45 (1984) C1-337.
- [7] A. Yamamoto, private communication.
- [8] M.A. Green et al., Operation of a two-phase cooling system on a large superconducting magnet, Proceeding of the Eighth International Cryogenic Engineering Conference, Genoa, Italy, June 1980, IPC Science and Technology Press, 1980, p. 72.
- [9] Th. Schneider and P. Turowski, Thirteenth International Conference on Magnet Technology, Victoria, Canada, September 1993, Paper R-J-07.
- [10] Bill Morse, Characteristic of the E821 Interconnects, GM2-doc-302-v1.
- [11] Bill Morse, Coil Resistance to Ground Measurements, GM2-doc-352-v1.
- [12] Bill Morse, Coil Resistance to Ground Measurements, GM2-doc-976-v1.
- [13] Del Allspach, Vacuum and Cryogenics Presentation at g-2 December 2012 Collaboration Meeting, GM2-doc-615-v1.
- [14] T. Tonogi et. al., Aluminum Stabilized Superconductor for the Atlas Central Solenoid Magnet, Hitachi Cable Review No. 18, V87.
- [15] Testing of Splice Resistance, DocDB 1884.
- [16] Magnetic Forces on Poles and Coils (Update), DocDB 1275.
- [17] Magnetic Forces on Yoke, DocDB 1334.

- [18] Magnetic Forces on Poles and Coils (Update), DocDB 1243.
- [19] Opera3D Simulation of Eddy Currents, DocDB 1417.
- [20] Effect of Eddy Currents on Mu of the Iron and Ground Loop Currents, DocDB 1391.
- [21] External Fields, Saturation, and Eddy Currents, DocDB 1152.
- [22] First Results of Cracks and Gaps in Opera3D, DocDB 765.
- [23] Opera3D Study of Misalignment, DocDB 1121.
- [24] Coil Displacement Study, DocDB 1410.
- [25] Alignment Effect on Precision Field, DocDB 1846.
- [26] Alignment and Metrology Update, DocDB 1748.
- [27] Alignment and Metrology Update, DocDB 1545.
- [28] Electrical Contractor drawings and Electrical Distribution for the Main Ring, Docdb 1654-v1.
- [29] Simplified Single-Line Electrical Drawings and for the Main Ring, Docdb 1654-v2.
- [30] Muon g-2 Grounding Strategy, DocDB 1858.
- [31] Muon g-2 Grounding Plan Drawing, DocDB 1882.
- [32] Rick Hance, "Dzero Solenoid Quench Protection and Operation", <http://www-d0.fnal.gov/hance/solenoid.htm>
- [33] Bruker Water System Proposal, DocDB 1916.
- [34] Bruker Power Supply Specification and Users Manual, DocDB 1917.
- [35] Muon g-2 Main Magnet Voltage Tap Illustration, DocDB 1914.
- [36] FPGA Based Quench Detection Systems, DocDB 1919.
- [37] Muon g-2 Magnet Ring Power Supply and Quench Protection, DocDB 1922.

